Aus der Abteilung für Hand-, Plastische und Ästhetische Chirurgie

der Ludwig-Maximilians-Universität München

Vorstand: Prof. Dr. Riccardo Giunta

Investigating the Reliability and Reproducibility of Nasal Anthropometry using Three-Dimensional Digital Stereophotogrammetry

Dissertation

zum Erwerb des Doktorgrades der Medizin

an der Medizinischen Fakultät der

Ludwig-Maximilians-Universität zu München

vorgelegt von

Zhouxiao Li

aus Wuhu, Anhui Provinz, China

2021

Mit Genehmigung der Medizinischen Fakultät

der Universität München

Berichterstatter: Prof. Dr. Riccardo Giunta

Mitberichterstatter: PD Dr. John Martin Hempel

Mitbetreuer durch den

promovierten Mitarbeiter: **Dr. Konstantin Koban**

Prof. Dr. Thilo Schenck

Dekan: **Prof. Dr. med. Thomas Gudermann**

Tag der mündlichen Prüfung: 15.12.2021

Eidesstattliche Versicherung

Ich erkläre hiermit an Eides statt,

dass ich die vorliegende Dissertation mit dem Thema

“**Investigating the Reliability and Reproducibility of Nasal Anthropometry using Three-Dimensional Digital Stereophotogrammetry**”

selbständig verfasst, mich außer der angegebenen keiner weiteren Hilfsmittel bedient und alle Erkenntnisse, die aus dem Schrifttum ganz oder annähernd übernommen sind, als solche kenntlich gemacht und nach ihrer Herkunft unter Bezeichnung der Fundstelle einzeln nachgewiesen habe.

Ich erkläre des Weiteren, dass die hier vorgelegte Dissertation nicht in gleicher oder in ähnlicher Form bei einer anderen Stelle zur Erlangung eines akademischen Grades eingereicht wurde.

München, 18.12.2021	Zhouxiao Li
_____	_____
Ort, Datum	Unterschrift Doktorandin/Doktorand

Die vorliegende Dissertation wurde nach § 4a der Promotionsordnung

(konsolidierte Fassung mit der 11. Änderungssatzung vom 15. September 2016 - gültig für alle Promotionsvorhaben, die durch Abgabe der Betreuungsvereinbarung bis zum 30.09.2018 offiziell im Promotionsbüro angemeldet wurden)

für die Medizinische Fakultät der Ludwig-Maximilians-Universität München gestaltet.

Table of Contents

List of Abbreviations **1**

Abstract **5**

1 Introduction **7**

1.1 The Development of 3D Imaging 7

1.1.1 3D Facial Imaging System 7
1.1.2 Commonly used 3D Imaging Technique 9

1.2 The Application of Facial 3D Imaging in Plastic Surgery 12

1.2.1 The Role of Facial 3D Imaging in Facial Measurement 12
1.2.2 Practical Application of 3D Imaging Technology in Rhinoplasty 13
1.2.3 Prospects for the Application of 3D imaging in Rhinoplasty 15

2 The Aim of this Study **16**

3 Materials and Methods **18**

3.1 Study Sample 18
3.2 3D Surface Imaging Device 19
3.3 Image Sampling Process 20
3.4 Processing 3D Images 21
3.5 Data Evaluation 23
3.6 The Reliability of the Landmarks 34
3.7 The Reproducibility of the Landmarks 35
3.8 Statistical Analysis 36

4 Results **37**

4.1 Reliability 37

4.1.1 Overall Reliability 37
4.1.2 Intra-rater Reliability of Landmarks 39
4.1.3 Inter-rater Reliability of Landmarks 41
4.1.4 Intra-method Reliability with VECTRA XT Imaging System 43

4.2 Reproducibility 45

4.2.1 Overall Reproducibility 45
4.2.2 The Landmarks' Reproducibility in Caucasian and Asian Participants 46
4.2.3 The Landmarks' Reproducibility in Female and Male Subgroups 49

4.3 The Representative Landmarks in Ethnic and Gender Subgroups 52

5 Discussion **55**

5.1 Study Design 55
5.2 Study Results 56
5.3 Significance 58
5.3.1 Consistence 58
5.3.2 Influencing Factors 59
5.3.3 Difference and Diversity 59
5.4 Limitations 61
6 Summary 62
7 References 63
8 Appendix 73
8.1 List of Figures 73
8.2 List of Tables 74
9 Attachment 75
9.1 Tables 75
10 Acknowledgement 86
11 Publications: 88

List of Abbreviations

2D = Two-dimensional

3D = Three-dimensional

3DSI = Three-dimensional Surface Imaging

Ac = Alar curvature

Al = Alare

C = Cervical

Cc = Columella constructed point

Cm = Columella

CT = Computed tomography

Em = Eyebrow margin

En = Endocanthion

G = Glabella

Hn = Highnasal

ICC = Intraclass correlation coefficient

Li = Labrale inferius

LMU = Ludwig-Maximilians-Universität München

Ln = Lownasal

Ls = Labrale superius

MAD = Mean absolute difference

Me = Menton

MR = Magnetic resonance

N = Nasion

Nb = Nostril base point

Nl = Nostril lateral point

Nm = Nostril medial point

Nt = Nostril top points

Pa = Postaurale

Pg = Pogonion

Prn = Pronasale

REM = Relative error measurement

rTEM = Relative technical error of measurement

Se = Sellion

Sl = Sublabiale

Sm = Supramental

Sn = Subnasale

Stb = Supratip break

Sto = Stomion

TDP = Tip defining point

TEM = Technical error of measurement

Trg = Tragus

Tri = Trichion

Zy = Zygion

Zusammenfassung

Die dreidimensionale Oberflächendarstellung (3DSI) hat sich zu einer etablierten Methode für anthropometrische Messungen entwickelt und wird in einer Vielzahl medizinischer Disziplinen angewendet, beispielsweise bei der Analyse der kindlichen Gesichtsentwicklung, bei der Analyse angeborener Erkrankungen wie Lippen-Kiefer-Gaumenspalten oder Veränderungen des Schädels, in der rekonstruktiven Gesichtschirurgie und zur ästhetischen Beratung in der Gesichtschirurgie. Als nicht-invasive Technologie spielt sie eine immer wichtigere Rolle bei der Beurteilung der Gesichtsmorphologie und wird häufig zur Unterstützung strahlungsintensiver CT-Bildgebung oder teurer MRT-Bildgebung eingesetzt. 3DSI des Gesichts ermöglicht detaillierte Messungen, einschließlich Entfernungen, Krümmungen, Volumen, Winkel und Oberflächen. Frühere Studien haben eine hohe Zuverlässigkeit bei der Anwendung von 3DSI für die Planung und Nachsorge in der Rhinoplastik und der Mund-Kiefer-Gesichtschirurgie Chirurgie gezeigt. Im Vergleich zu den validierten Daten in der umfangreichen Literatur zur Periorbitalregion fehlen validierte Daten zur 3D-Erfassung im Nasenbereich. Daher ist eine unabhängigere Überprüfung der abgeleiteten 3D-Messungen erforderlich. Ziel der vorliegenden Arbeit ist es, durch die Evaluierung der Zuverlässigkeit und Reproduzierbarkeit der neuartigen digitalen 3D-Nasenanthropometrie den Grundstein für eine breite Anwendung zu legen. In dieser Studie wurden standardisierte 3DSI von 160 Freiwilligen (80 europäische Kaukasier und 80 Asiaten) unter Verwendung des etablierten Vectra 3D-Bildgebungssystems durchgeführt. Zwei Untersucher erstellten in getrennten Sitzungen wiederholt 3D-Bilder der Gesichtsregionen der Freiwilligen. 46 Weichteil-Landmarken wurden festgelegt und ihre 138 Koordinaten in drei räumlichen Ebenen (x-y-z-Achse) bestimmt. 57 entsprechende projektive lineare Distanzen, Oberflächendistanzen, Winkel und

Gesichtsverhältnisse wurden auf die Zuverlässigkeit von Intra-Rater, Inter-Rater und Intra-Methode überprüft. Die statistische Analyse der Reliabilität erfolgte mittels mittlerer absoluter Differenz (MAD), relativer Fehlermessung (REM), technischer Messfehler (TEM), relativer technischer Messfehler (rTEM) und Intraklassenkorrelationskoeffizient (ICC). Vier Klassen von ICC wurden gemäß dem Konsens definiert: < 0,5, schlecht; 0,5 bis 0,75, mäßige Zuverlässigkeit; 0,75 bis 0,9, gute Zuverlässigkeit; ≥ 0,9, ausgezeichnet. Die Reproduzierbarkeit der Landmarkenkoordinaten wurde in drei Kategorien (< 0,5 mm, < 1 mm und > 1 mm) sowohl für die Intra- als auch für die Inter-Rater-Reproduzierbarkeitsbewertungen eingeteilt. Insgesamt sind die 46 Landmarken und die darauf basierende Anthropometrie in dieser Studie gut vergleichbar. Die Reproduzierbarkeit für 138 Koordinaten in 160 Proben verteilt sich wie folgt: Intra-Rater: < 0,5 mm (45%), < 1 mm (42%), > 1 mm (13%); Interrater: < 0,5 mm (31,2%), < 1 mm (42%), > 1 mm (26,8%). Die Reproduzierbarkeit von Landmarken in der Nasenspitzenregion ist zwischen Kaukasiern und Asiaten leicht unterschiedlich. Die Landmarken im Lippen- und Kinnbereich sind bei Männern im Vergleich zu Frauen im Allgemeinen besser reproduzierbar. Es gibt jedoch keinen Unterschied in der Reproduzierbarkeitsrangfolge von Landmarken nach Geschlecht. Darüber hinaus zeigen alle 57 Messungen eine gute Reliabilität mit ICC über 0,75. Davon zeigen 41 Messungen eine ausgezeichnete Zuverlässigkeit mit einem ICC größer oder gleich 0,9. Der MAD beträgt für die meisten geradlinigen Entfernungen weniger als 0,3 mm. Alle MAD-Winkel sind kleiner als 0,3 Grad. Der MAD liegt bei Ratio-Messungen unter 0,01, mit Ausnahme von Nostril Aspect Ratio left (0,013). 50 Messungen der Schätzungen für die relative Fehlergröße lagen unter 1 %. Alle rTEM-Schätzungen waren von sehr guter Reliabilität.

Abstract

Three-dimensional Surface Imaging (3DSI) becomes an established method for anthropometric measurements and is applied in a variety of medical disciplines, for example, in the analysis of infant facial development, in the analysis of congenital conditions such as cleft lip and palate or alterations of the skull, in facial reconstructive surgery, and for aesthetic facial plastic surgery consultation. As a non-invasive technology, it plays an increasingly important role in evaluating facial morphology and is often used in support of radiation-intensive CT imaging or expensive MRI imaging. 3DSI of the face provides detailed measurements including distances, curvatures, volumes, angles, and surface areas. Previous studies have shown considerable reliability in the application of 3DSI for the planning and follow-up in rhinoplasty and craniomaxillofacial surgery. Compared to the validated data in the extensive literature on the periorbital region, there is a lack of validated data for 3D acquisition in the nose area. Therefore, more independent verification of the 3D derived measurements is necessary. The present thesis aims to lay the foundation for extensive application of the novel 3D digital nasal anthropometry by evaluating its reliability and reproducibility. In this study, standardized 3DSI of 160 volunteers (80 European Caucasian and 80 Asians) was performed using an established Vectra 3D imaging system. Two raters 3D-imaged the volunteers' facial regions in separate sessions repeatedly. 46 soft-tissue landmarks were determined, and their 138 coordinates were recorded in three spatial planes (x-y-z axis). 57 corresponding projective linear dimensions, surface distances, angles and facial ratios were evaluated for the reliability of intra-rater, inter-rater, and intra-method. Statistical analysis for the reliability was done through mean absolute difference (MAD), relative error measurement (REM), technical error of measurement (TEM), relative technical error of measurement (rTEM), and intraclass correlation coefficient (ICC). Four

classes of ICC were defined according to the consensus: < 0.5, poor; 0.5 to 0.75, moderate reliability; 0.75 to 0.9, good reliability; ≥ 0.9, excellent. The reproducibility of landmarks coordinates was divided into three categories (< 0.5 mm, < 1 mm, and >1 mm) for both intra- and inter-rater reproducibility assessments. Overall, the 46 landmarks and the anthropometry based on them are highly comparable in this study. The reproducibility for 138 coordinates in 160 samples distribute as follows: intra-rater: < 0.5 mm (45%), < 1 mm (42%), > 1 mm (13%); inter-rater: < 0.5 mm (31.2%), < 1 mm (42%), > 1 mm (26.8%). The reproducibility of landmarks in the nasal tip region is slightly different between Caucasians and Asians. The landmarks in the lip and chin area of males are more reproducible compared with females generally. However, there is no difference in the reproducibility ranking of landmarks by genders. Furthermore, all 57 measurements display a good reliability with ICC above 0.75. Of these, 41 measurements show excellent reliability with ICC larger than or equal to 0.9. The MAD is less than 0.3 mm for most straight-line distances. All the MAD of angles are smaller than 0.3 degree. The MAD is less than 0.01 for ratio measurements except for Nostril Aspect Ratio left (0.013). 50 measurements of estimates for the relative error magnitude were less than 1%. All of rTEM estimates were of very good reliability.

1 Introduction

1.1 The Development of 3D Imaging

In 1955, Sassouni[1] first described a method for capturing faces in three dimensions: he projected a pattern onto the face and photographed it from a 90-degree angle. This method was further developed by Cobb[2] in 1971 and further optimized in 1976 and 1983 respectively[3-4]. They projected a pattern bilaterally onto the patient with two projectors and took frontal images. In 1971, Burke and Beard[5] proposed a stereographic procedure. They took two images from different angles, and the images were then viewed under special equipment to obtain the depth information required. Beckman *et al*.[6] presented a study that also involved the 3D recording of the facial soft tissue surface in 1985. He proposed a clinically applicable method for the first time, which allowed the soft tissue surface of the face to be captured in three dimensions with the help of a computer and to be displayed in the sagittal and horizontal plane.

Since entering the 21st century, 3D stereoscopic photography system has made great progress. With the wide application of optical sensors, the image resolution of 3D photography has also improved significantly. In contrast to 2D soft tissue analysis, reference points can be set and defined in a display of the face in sagittal, transverse and vertical directions[71-75].

1.1.1 3D Facial Imaging System

In recent years, 3D facial imaging has become well known due to its use in security systems and facial recognition, animation production, virtual reality and other fields. This

technique has also been widely used in clinical medicine, especially in the field of plastic surgery. A majority of clinically used facial 3DSI systems are based on digital stereophotogrammetry and are able to accurately reflect the facial contours and reproduces the skin color and texture realistically. Its advantages are fast acquisition time, wide surface coverage, and a non-invasive and radiation-free technique[7].

3D facial photography systems consist of a dedicated camera and computer with software solution. These systems can be divided into active, passive and hybrid stereophotogrammetry techniques regarding the use of its light source[7]. The active system needs to emit a certain pattern structured light onto the target object, from which it calculates and extracts the projection information of the object to generate a 3D surface model. The system does not require an additional light source, avoiding the interference of disturbing light. It also allows for better reconstruction of darker 3d images of objects but with longer sampling times. One representative of this technology is the Artec Eva (Artec 3D, Luxembourg), a handheld active 3D camera system with high accuracy and portable size. It has full 360-degree capture range and be used for photography of any part of the body[8,30].

Passive photogrammetry can be divided into monocular vision, binocular vision, and multi-eye vision methods according to the number of cameras. This 3D reconstruction is based solely on the number of images taken with the cameras without a specific light grid pattern. The method is therefore highly dependent on the quality and resolution of the camera and needs to capture as much of the target's characteristic information as possible. In addition, lighting conditions in the environment should be strictly controlled during photography to minimize the impact of ambient spectral reflections. The external lighting conditions also need to be tightly controlled to reduce glare. The widely used passive 3D photography system in clinical medicine is the Canfield Vectra series (Canfield Sci., Parsippany, USA). They can capture image fast and easily using high-

resolution cameras[9].

Hybrid systems combine the first two technologies. The main series in used is the 3dMD system, which consists of six machine vision cameras with 1.5 ms capture speed at highest resolution. But the system requires the user to calibrate it each time before using[7].

The two main indicators of the accuracy of a 3D stereo camera system are reproducibility and absolute accuracy. In a comparison between direct, 2D anthropometry and the Vectra system for 24 periocular landmarks on 46 Caucasian individuals showed that the 3D stereophotogrammetry based Vectra system yield high accuracy and very good reliability[10]. Many commercially available 3D surface imaging systems showed high reproducibility and reliability[11-14].

1.1.2 Commonly used 3D Imaging Technique

Objective and comprehensive craniofacial soft tissues measurements provide a quantitative basis for surgeons' consultation, as well as to preoperative and postoperative effect comparison and follow-up[15-18]. In craniofacial anthropometry, the advances of the last decades have combined the objective, yet mostly 2D, common and direct anthropometric examinations with tape measure, calliper, and angular measurement, with subjective 2D photography. 2D photogrammetry has been widely applied to evaluate rhinoplasty outcomes such as nasal tip position, nasal alare width, and nostril shape, as well as in nasal analysis in various ethnics[19-20]. However, a significant amount of time is required for a detailed recording of the complexity of the nose[21-23]. 3DSI becomes an established method for anthropometric measurements and is applied in a variety of medical disciplines, for example, in the analysis of infant facial

development, in the analysis of congenital conditions such as cleft lip and palate or alterations of the skull, in facial reconstructive surgery, and for an aesthetic facial plastic surgery consultation[24-27]. As a non-invasive technology, it plays an increasingly important role in evaluating facial morphology and is often used in support of radiation-intensive CT imaging or expensive MRI imaging. Although there are numerous devices for 3D acquisition, the basis of anthropometric surveying is a landmark-based approach normally. Facial surface landmarks are critical to the accuracy of 3D facial morphology measurement and analysis[28-29]. 3DSI of the face provides detailed measurements including distances, curvatures, volumes, angles, and surface areas[30-31]. 3D reconstruction of the patient's nose can reflect the actual nasal anatomy and adjacent tissue relationships. The common techniques can be simply divided into two categories: computer-aided 3D reconstruction and direct 3D imaging. The former refers to the use of multi-directional 2D images obtained from X-rays, ultrasound, CT, MR and photography to reconstruct a 3D image via specific algorithms; the latter refers to contactless one-time stereoscopic imaging techniques[32].

1.1.2.1 Computer-aided 3D Imaging

(1) X-ray: 2D images of the head and face are taken anteroposteriorly, bilaterally using X-rays, and the bony landmarks are manually marked to construct the 3D image. Its use is limited by the presence of radioactivity, the tedious manual pointing process, and the inability to reproduce soft tissue structures[33].

(2) 3D-ultrasound: inexpensive, also allows extraction of specific echogenic tissue. The imaging of specific echogenic tissues is widely used in clinical practice. However, the probe can cause compression of soft tissue during imaging, interfering with accurate reproduction[33].

(3) 3D-CT: As the most mature and commonly used technique in this field, 3D-CT is

used to visualize and reconstruct the head and face in three dimensions by fitting the tomography results to the external surface and the internal anatomy, allowing a full view from any angle by rotation, and extracting local images of specific tissue structures. The limitations of this method are that the thickness of the tomogram can lead to a partial loss of information and that it is somewhat radioactive and not suitable for frequent follow-up[33].

(4) 3D-MR: 3D-MR provides significantly better resolution of soft tissues than CT and is non-radioactive. However, it is not suitable for patients with metallic facial prostheses and has the disadvantages of being noisy, confined and slow[33].

(5) 3D photographic compositions: Synthesize three-dimensional images using planar images taken by camera, which is easy to operate and low in cost. However, factors such as light and lens distortion affect the accuracy of restoration[33].

1.1.2.2 Direct 3D Imaging

(1) Moiré fringes measurement: Based on the moiré effect, arbitrary profiles and stereo fluoroscopic images are obtained with the aid of contour stripe maps, which can be used for dynamic expression reproduction and surgical documentation[34]. The technique is applicable to relatively smooth facial area, and slight changes in head position can have a significant impact on the imaging data[35].

(2) Laser triangulation: This means scanning the object with laser points or strips, receiving the return information to produce a stereo image based on triangulation. The entire imaging process takes approximately ten seconds, and the target object must keep relatively stationary during photography. To protect the eyes, patients must close their eyes or use protective goggles[36].

(3) Structured light technique: The deflection of the infrared light reflects the local loci of depth-of-field information, superimposed on the flat information of the 2D image, to

achieve 3D imaging[37]. This technology is used for face recognition in cutting-edge mobile devices, but it is difficult to detect the deep tissue structures that are covered[38-39].

(4) Stereophotogrammetry system: The superimposed imaging of the binocular vision system produces stereo vision. Based on this principle, stereophotogrammetry uses multiple cameras to produce a 3D image with the advantage of fast imaging in milliseconds[40]. This technology is particularly suitable for small-scale, high-precision visualization of the face, where accurate and realistic images can be used to aid pre-operative patient communication and surgical planning[41].

1.2 The Application of Facial 3D Imaging in Plastic Surgery

1.2.1 The Role of Facial 3D Imaging in Facial Measurement

Previous direct anthropometric measurements were mainly conducted with the use of tape ruler and calipers. This measurement requires direct contact with the patient and the patient needs to remain stationary for a few minutes, which is often difficult and time-consuming especially in younger children but depending on the amplitude of measurements taken. In traditional photography, 2D photos often fail to reflect the characteristics of the 3D structure of patient, and they often only reflect changes in facial profile while ignoring overall and frontal changes when 2D photos are applied to facial simulation prediction. The facial 3D photo provided by the facial 3D photography system can truly reflect the characteristics of the soft tissues of the research object and can be

used for 3D digital analysis. The addition of 3DSI overcomes the limitations of 2D planar images, making preoperative evaluation, treatment plan formulation, and doctor-patient communication more convenient and efficient[42].

Currently, 3DSI is a promising tool in the assessment of facial soft tissue morphology for clinical practice. Its advantage lies in the swift collecting of digital information and high-resolution 3D images, which can truly reflect the facial skin color and surface texture of the subject[43-44]. The modelled 3d image can be easily archived and can be applied for complex measurements such as angles and curvatures through an indirect approach. The technique could be used for several fields such as the evaluation of facial development during children's growth, analysis of facial morphology of patients affected by congenital and acquired pathological factors, quantitative analysis of facial changes of patients undergoing facial cosmetic, reconstructive, and orthodontic surgery, and morphological study on the normalization of facial impairments[45-48].

3D images are mainly used for anthropometry based on facial soft tissue landmarks. Because the placement of landmarks is based on images instead of direct physical evaluation, so the verification of the reliability and reproducibility of soft-tissue landmarks is essential for cephalofacial measurement using 3D photogrammetry system[4,8,10-13].

1.2.2 Practical Application of 3D Imaging Technology in Rhinoplasty

In plastic surgery treatment, facial soft tissue is a very important factor especially for rhinoplasty. The nose has a subtle local anatomical structure with large individual differences. The plastic surgeon needs to conduct a preliminary assessment of nasal

condition of the patient through visual and physical assessment during face-to-face consultation initially. The information of internal and external anatomical structure of the body can be further obtained by means of imaging. Currently, 3D imaging technology is mainly used for pre-operative assessment, simulation, and post-operative follow-up of rhinoplasty. The use of 3D imaging provides a precise 3D display of the patient's nasal face, allowing the surgeon to visualize the relevant anatomical information and to communicate with the patient in an effective preoperative manner. Direct 3D imaging allows for a faster visualization of the external display of the nasal face, while 3D-CT/MR allows for the reconstruction of the internal nasal tissues. More importantly, the model parameters can be adjusted to simulate and compare different surgical outcomes, helping to determine the optimal surgical solution[49]. From the patient’s point of view, 3D imaging can assist them in establishing reasonable surgical expectations so that they can understand surgical options and associated risks better. The study has shown that patients who use 3D imaging are more aware of and are ultimately more satisfied with the results of their plastic surgery operations[42]. 3D imaging also plays an important role in post-operative follow-up as it can be overlaid directly with the pre-operative 3D imaging to provide a visual display of the surgical outcome with precise feedback on subtle changes. It not only helps to improve patient satisfaction after surgery but also allows the surgeon to choose the right time for any necessary secondary repair[50-51]. With the improvement of the 3D imaging assessment method, the application of this technology will become more standardized before and after rhinoplasty , which will help its promotion in clinical practice further.

1.2.3 Prospects for the Application of 3D imaging in Rhinoplasty

At this stage, the application of 3D imaging technology is still limited to the scope of the assessor. It is difficult for patients to articulate their surgical expectations in a short period so that physicians inevitably make judgements based on their own subjective experience, there is also a lack of patient communication and follow-up with the increasing number of outpatients. The idea of involving patients in all aspects of rhinoplasty pre- and post-surgery can help to resolve the conflicts, and this can only be achieved with the development and dissemination of mobile 3D imaging technology[52]. The so-called mobile 3D imaging technology is a portable device that enables stereoscopic imaging and simultaneous translation of information[53]. It is now possible to obtain a 2D image of a patient's nasal face using a mobile phone or computer and then use an application with a pre-defined 3D imaging algorithm to help the patient obtain a simple 3D nasal and facial image[54]. The simultaneous transformation enables the corresponding anatomical data to be fed back when the stereo images are locally adjusted[55]. In this way, patients have a more intuitive understanding of their anatomical conditions and can easily make adjustments and ultimately achieve a satisfactory outcome. It allows for more efficient patient-physician communication through visualization and digitization of the desired surgical outcome. Post-operative follow-ups can be carried out anywhere and anytime with the aid of mobile 3D imaging devices, making it even easier for both the patient and the doctor. After obtaining the consent of patients, the mobile imaging data can be aggregated and shared with the platform, enabling remote physician selection, specialist consultations and pre-operative discussions[55].

2 The Aim of this Study

Over the last few decades, 3D imaging has developed at a rapid pace. It allows for more precise determination of spatial measurement points and enables more accurate calculation and interpretation of angles and distances, enabling comprehensive soft tissue-based anthropometry.

Previous studies have shown considerable reliability in the application of 3DSI for the planning and follow-up in rhinoplasty and craniomaxillofacial surgery. While a large number of studies are dedicated to the acquisition of the entire face, there are only a few studies dedicated to the complexity of individual areas. Compared to the validated data in the extensive literature on the periorbital region[56], there is a lack of validated data for 3D acquisition in the nose area. Facial surface landmarks are critical to the accuracy of 3D facial morphology measurement and analysis. Although there has been profound research on the reliability and repeatability of landmarks on facial 3D images, they are only concentrated in the same race and the sample size included is relatively small. Additionally, many of them did not address the issue of reproducibility, and most of the selected landmarks were traditional reference points that had been validated[57-59]. Any facial morphological analysis based on anatomical landmarks requires highly reproductive and novel reference points across different populations. Therefore, we conducted this study based on the current literature.

The present thesis introduces several well-described landmarks to an established portfolio of 3D derived landmarks and measurements in order to ensure standardized and accurate coverage of the nasal area. Nevertheless, different facial structures are inconsistent due to their particular depth, contour and shape. Therefore, the reliability

and reproducibility of these facial soft tissue landmarks associated with nasal anthropometry and their corresponding measurements should be validated before their application in clinical practice.

The aims of the present thesis are:

1. Investigating the reliability of the identified facial landmarks used in this study.
2. Determining the average values for the nasal measurements based on the facial landmarks.
3. Verifying the reliability of nasal measurements.
4. Investigating the reproducibility of the facial landmarks position on three spatial planes in Caucasian and Asian groups.

3 Materials and Methods

3.1 Study Sample

The study involved 80 European Caucasians (40 males, 40 females) and 80 Asians (40 males, 40 females). The age of Caucasian volunteers ranged from 20 to 50 years old (30.49 ± 5.52 years). The age of Asian volunteers ranged from 18 to 45 years old (30.36 ± 2.99 years) **(Table 1)**. Written informed consent was acquired before enrollment. The study was approved by the local university ethical committee (REF: 266-13) and conducted according to the Declaration of Helsinki. Exclusion criteria were facial malformations, previous facial surgery, and volunteers diagnosed with epilepsy or other seizure disorders.

Table 1. Demographic characteristics of study participants

Age	Males (n=80)	Females (n=80)
Mean ± SD	31.36±4.68	29.50±3.97
Range	23 - 50	20 - 41
18-23 years	1	6
24-29 years	28	36
30-35 years	37	32
36-41 years	12	6
>42 years	2	-
Race		
Caucasian	40	40
Asian	40	40

3.2 3D Surface Imaging Device

The Vectra XT 3D Surface Imaging System (Canfield Inc., New Jersey, USA) is a three-pod passive stereo photogrammetry system with six cameras at a fixed position specially created for the health care sector. It is a fully automated digital 3D stereoscopic measuring device capable of 3D high-resolution color surface capture of face in 3.5ms, which limits the risk of motion artifacts. Its proprietary lighting system automatically adjusts the focal length for optimal face imaging **(Figure 1)**. For our study, it served as the 3D imaging system based on its widespread usage in clinical and research[10,27,30-34,56].

Figure 1. Vectra XT 3D Surface Imaging System

3.3 Image Sampling Process

Before taking the photo, any factors that would interfere with the image modelling, such as jewelry, glasses, and clothing elements (scarves, hat, etc.), were removed from the volunteers. They were asked to remove any hair from the face, forehead, and ears to fully expose the facial area. Male volunteers were asked to shave because the beard creates artifacts for the image. The scan was carried out in a room illuminated by fluorescent lights. All volunteers were asked to sit on the same chair remaining their lips closed without grinding the teeth, and look directly at the red marker dot on the 3D camera with a neutral facial expression and a natural head position. Light conditions and the background were not specifically changed in our consultation room, to achieve conditions similar to our daily routine **(Figure 2)**. A session consisted of 3D scans with each rater.

Figure 2. The standard position for an image capture with the Vectra XT

3.4 Processing 3D Images

All captured images were processed, aligned, and analyzed with proprietary Mirror® (Canfield Scientific; NJ, USA). The software has also been implemented for providing reference frameworks of the x-, y-, z-axis (sagittal, Y-Z plane; coronal, X-Y plane; and transverse, X-Z plane) so as to automatically standardized by unifying orientation for different images. The entirety of the face was marked, and symmetry in the planes were automatically adjusted by the integrated software. The midpoint between two endocanthions were chosen (mid-intercanthal point) as the origin point. The sagittal plane was referenced to the origin passing through the midline of face, the coronal plane is determined to be the average natural head position, and the transverse is established to span the origin **(Figure 3)**. The 3D face images were standardized on three planes to obtain comparable X, Y, and Z coordinates to evaluate the reproducibility of facial landmarks[60-61].

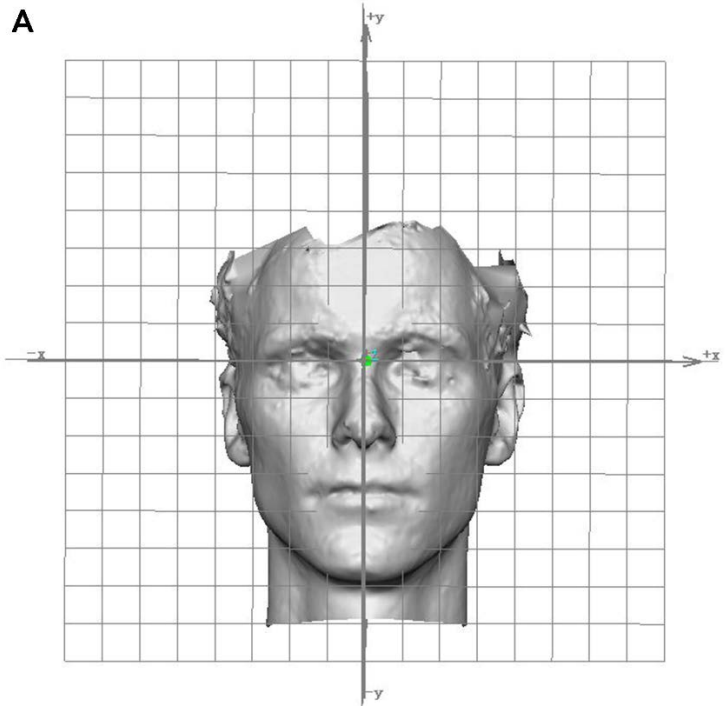

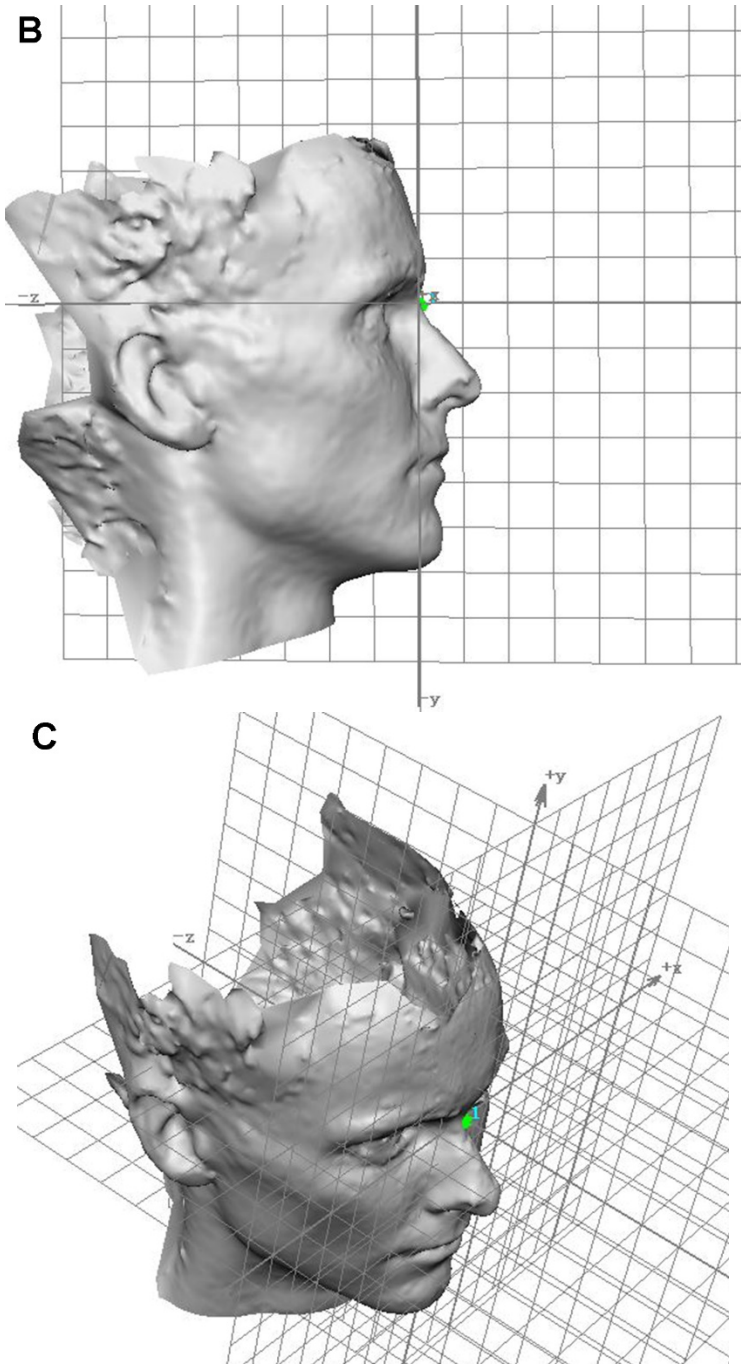

Figure 3. The standard position for an image capture with the Vectra XT 3D from frontal (A), right lateral (B), and right oblique (C) view.

3.5 Data Evaluation

In clinical routine of facial surgery, a variety of anatomical landmarks and clinical measurements can be performed. We used validated anatomical landmarks to obtain a wide range of 2D and 3D measurements. For each subject, 46 standardized facial landmarks **(Figure 4 to Figure 7)** were placed with the Mirror application (Canfield Scientific; NJ, USA). The definitions and descriptions of 46 landmarks are shown in **Table 2**. Landmark positions were defined according to Farkas, Swennen, and former nasal studies[62-65]. Two raters placed them separately on 3D facial images, and all landmarks' coordinate of X,Y,Z axes were recorded. The duplicability of landmarks designation, marker locating, and data collection procedure were previously reported, and found to be reliable. Subsequently, measures were performed for four types of measurements: 27 projective linear distances, two surface linear distances, eighteen angles, and ten ratios **(Table 3,Figure 8-10)**. Both raters are professional experienced researchers on 3D image anthropometry in our department. We performed two sets of photography for each volunteer at approximately one-hour intervals and recalibrated before the second set of photography. Each rater made the first-time evaluation on 3D images of volunteers (session1) using the VAM software and made another evaluation at least 24 hours later individually (session2).

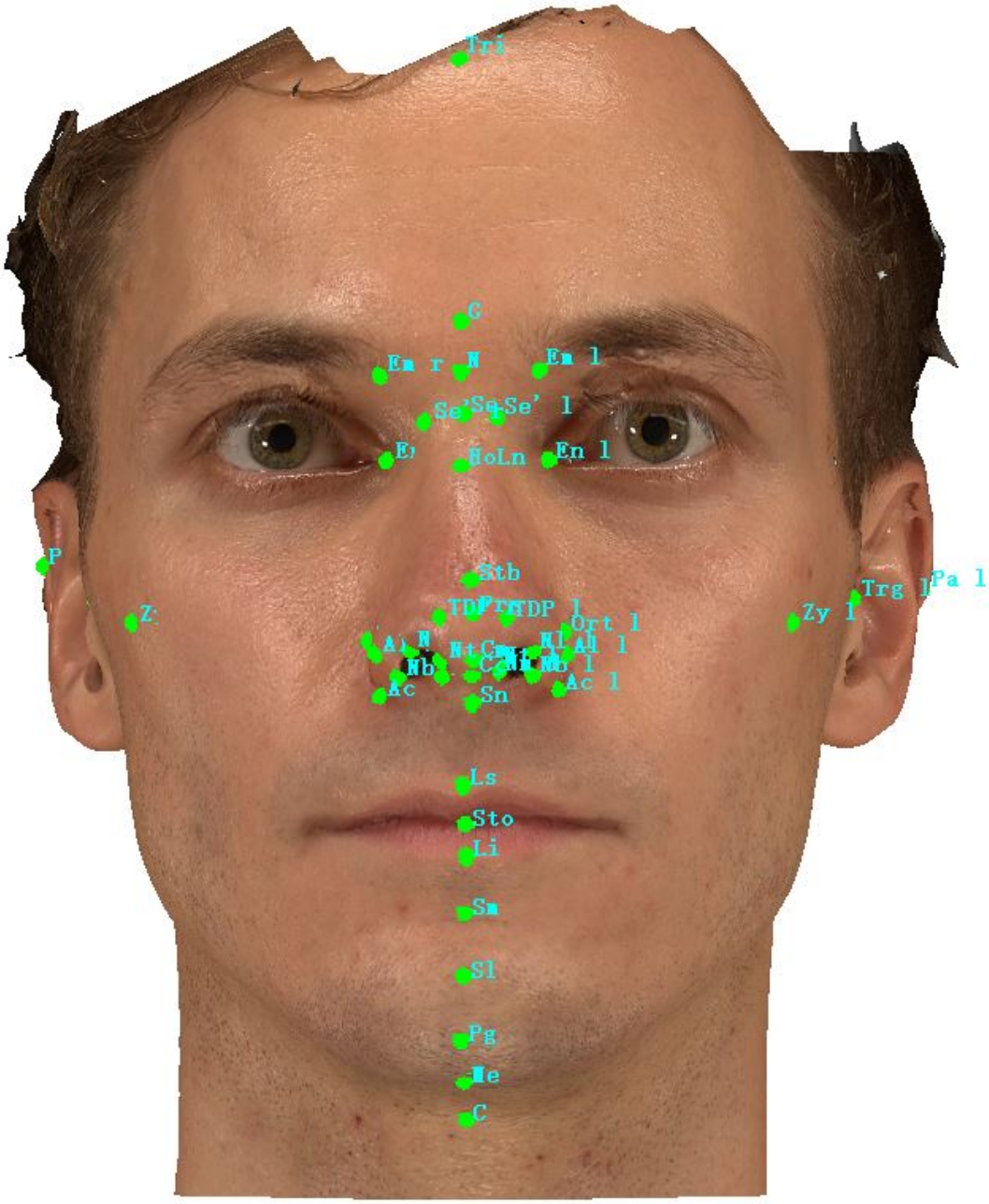

Figure 4. Illustration of the landmarks used in this study (front view)

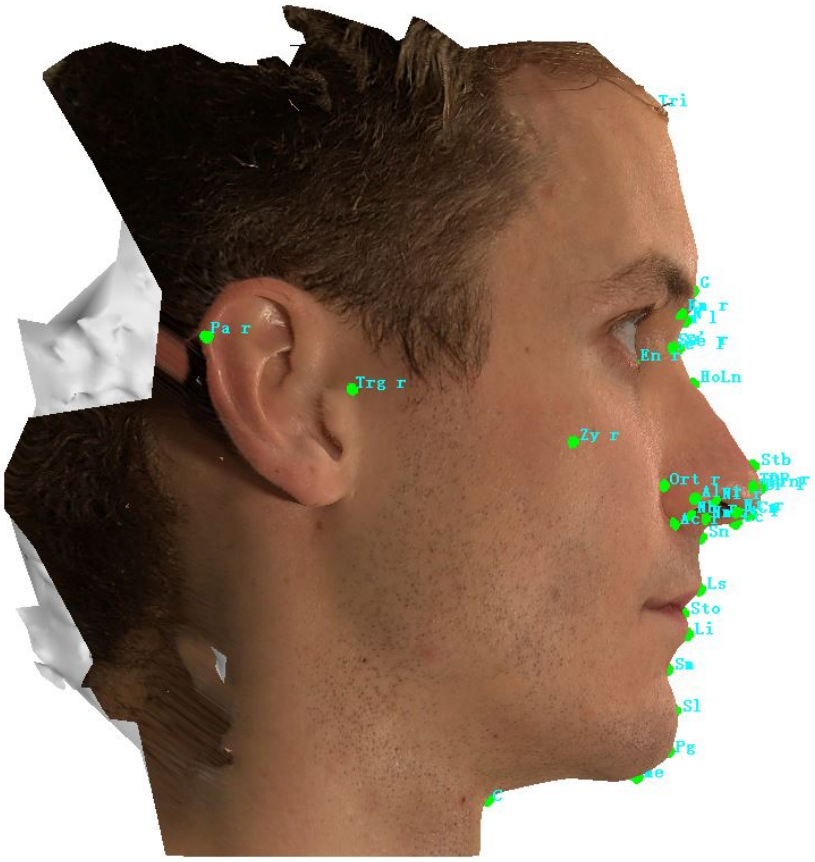

Figure 5. Illustration of the landmarks used in this study (isometric view)

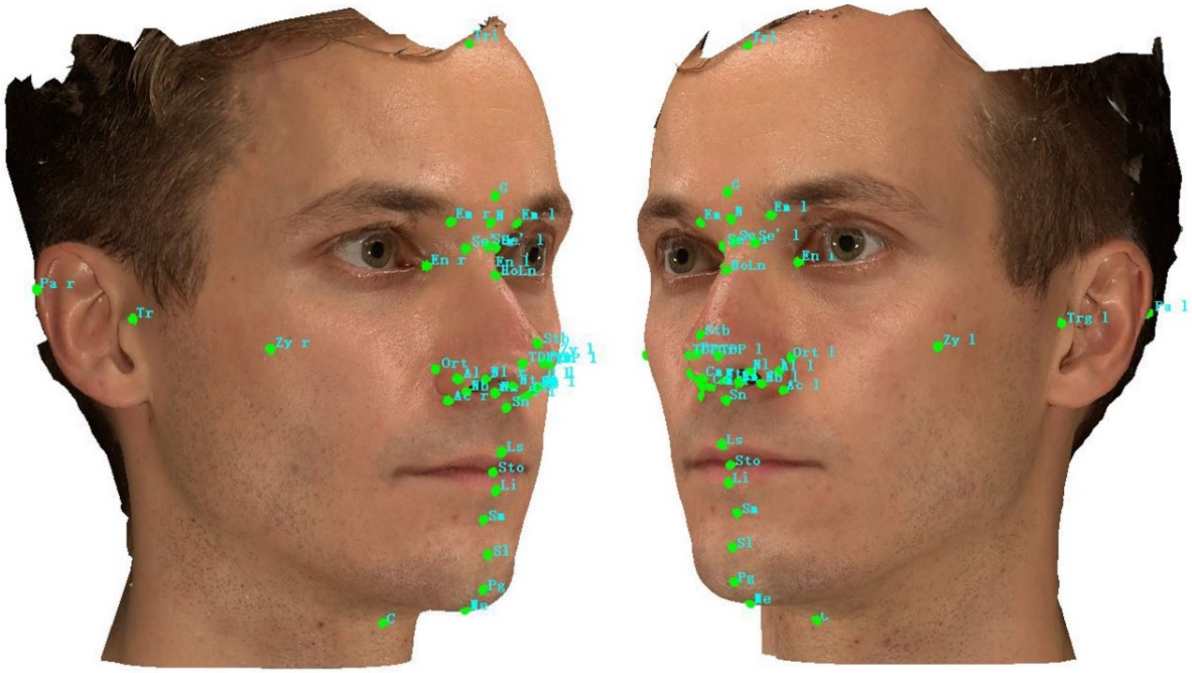

Figure 6. Illustration of the landmarks used in this study (bilateral view)

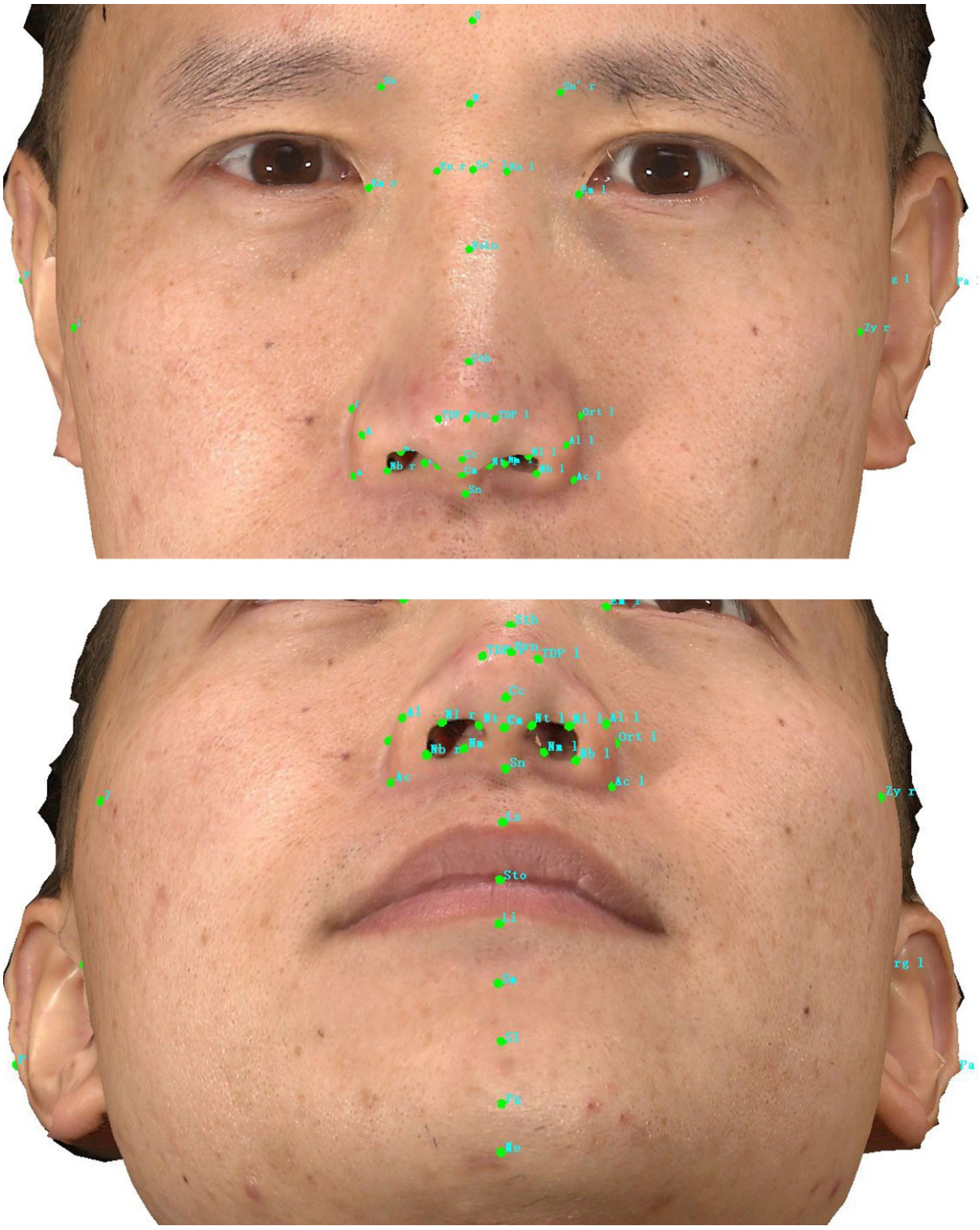

Figure 7. Illustration of the landmarks used in this study (local perspective)

Table 2. The name and definition of facial landmarks used in this study

Facial area	Landmarks	Definition
Eye	Em left	Lower margin of the left medial eyebrow end
	Em right	Lower margin of the right medial eyebrow end
	Endocanthion left (En l)	the left inner commissure of the palpebral fissure, the right midpoint of the frontonasal suture
	Endocanthion right (En r)	the right inner commissure of the palpebral fissure, the right midpoint of the frontonasal suture
Nose	Alar curvature / Alar crest left (Ac l)	Alar curvature point (ac) is the point located at the facial insertion of left alar base.
	Alar curvature / Alar crest right (Ac r)	Alar curvature point (ac) is the point located at the facial insertion of right alar base.
	Alare left (Al l)	the most lateral point on left alar contour
	Alare right (Al r)	the most lateral point on right alar contour
	Columella (Cm)	Most anterior and inferior point on apex of nose
	Columella constructed point (Cc)	the midpoint of the columella crest at the level of the nostril top points
	Glabella (G)	Most anterior point on midline of forehead
	Highnasal (Hn) or Lownasal (Ln)	the most anterior or posterior point on dorsum of nose between its root and tip
	Nasion (N)	Deepest point in middle of frontonasal curve
	Nostril base point left (Nb l)	the lowest point of each nostril or the inferior terminal point of left nostril axis.
	Nostril base point right (Nb r)	the lowest point of each nostril or the inferior terminal point of right nostril axis.
	Nostril lateral point left (Nl l)	the junction point of nostril short axis and the lateral margin of left nostril
	Nostril lateral point right (Nl r)	the junction point of nostril short axis and the lateral margin of right nostril
	Nostril medial point right (Nm l)	the junction point of nostril short axis and the medial margin of left nostril
	Nostril medial point right (Nm r)	the junction point of nostril short axis and the medial margin of right nostril
	Nostril top points left (Nt l)	the highest point of each nostril or the superior terminal point of left nostril axis.
	Nostril top points right (Nt r)	the highest point of each nostril or the superior terminal point of right nostril axis.
	Ort left	the left Junction of true vertical (TV) and true horizontal (TH) on the alare
	Ort right	the right Junction of true vertical (TV) and true horizontal (TH) on the alare
	Pronasale (Prn)	Most prominent point on apex of nose
	Sellion (Se)	the most posterior point of the frontonasal soft tissue contour in the midline of the base of the nasal root.
	Sellion' left (Se' l)	the left intersections of TH[Se] and Dorsal aesthetic lines

	Sellion' right (Se' r)	the right intersections of TH[Se] and Dorsal aesthetic lines
	Subnasale (Sn)	Deepest point in nasolabial curvature
	Supratip break (Stb)	the joint point of the dorsum and nasal tip
	Tip defining point left(TDP l)	the left most anterior projection of the tip cartilages, usually corresponding to the apex of the lobular arch anatomically
	Tip defining point right (TDP r)	the right most anterior projection of the tip cartilages, usually corresponding to the apex of the lobular arch anatomically
Mouth	Cervical (C)	Deepest point at angle of chin and neck
	Labrale inferius (Li)	Lower lip vermilion border
	Labrale superius (Ls)	Upper lip vermilion border
	Menton (Me)	Most inferior point on inferior edge of chin
	Stomion(Sto)	the midpoint of the horizontal labial fissure
	Sublabiale(Sl)	the most posterior midpoint on the labiomental soft tissue contour that defines the border between the lower lip and the chin.
	Supramental (Sm)	Deepest point in inferior sublabial concavity
	Pogonion (Pg)	Most anterior midpoint of chin
Ear	Postaurale left (Pa l)	Most posterior point on the free margin of the left ear
	Postaurale right (Pa r)	Most posterior point on the free margin of the right ear
	Tragus left (Trg l)	Most posterior point of auricular tragus left
	Tragus right (Trg r)	Most posterior point of auricular tragus right
Others	Trichion(Tri)	Intersection of hairline and midline of forehead
	Zygion left (Zy l)	the most lateral point on the outline of left zygomatic arch
	Zygion right (Zy r)	the most lateral point on the outline of right zygomatic arch

Table 3. List of 57 Nasal Measurements

Measurements	Abbreviation	Landmarks or definitions
Projective linear dimensions (Straight line distance)		
Face width	FW	Zy(l)-Zy(r)
Face width2	FW2	Postaurale(l)-Postaurale(r)
Face length	FL	Tri-Me
Nasal root width	NRW	Em(l)-Em(r)
Inner intercanthal distance	EnD	En (l)-En (r)
Sellion-Subnasal	SSn	Se-Sn
Dorsal bridge width (narrowest)	DBW	Se'(l)-Se'(r)
Nasal length	NL	G-Sn
Nasion-Alare*	NAL	N-Al
Dorsum length	DL	Se-Prn
Alar base width	ABW	Al(l)-Al(r)
Nasal base width	NBW	Ac(l)-Ac(r)
Alare length	ALL	Prn-Ac
Tip width	TW	TDP(l)-TDP(r）
Tip length	TL	Stb-Cm
Nasal Septum length	NSL	Cm-Sn
Pronasale-Columella	PRC	Prn-Cm
Nostril long Axis length	NLA	Nt-Nb
Nostril short Axis length*	NSA	the shortest distance perpendicular to the nostril long axis
Subnasal-Stomion	SSt	Sn-Sto
Subnasal-Menton	SMe	Sn-Me
Stomion-Menton	StM	St-Me
Columella-Subnasal	CSn	Cm-Sn

Surface linear distance		
Glabella-Nasion-Sellion	GNS	G-N-Se
Dorsum surface length	DSL	Se-stp-prn
Angles		
Nasalfrontal Angle	NFRA	G-Se-Prn
Nasolabial Angle	NLAn	Cm-Sn-Ls
Nasal Dorsum Angle	NDA	Se-Hn-Prn/Se-Ln-Prn
Vertical nasal angle	VNA	Prn-Se-Ort
Nasal Angle	NA	Sn-Prn-Se
Superior facial third Angle	SFA	Tri-Trg-Se
Middle facial third Angle	MFA	Se-Trg-Sn
Inferior facial third Angle	IFA	Sn-Trg-Me
Total facial convexity Angle	TFCA	G-Prn-Pg
Facial convexity Angle	FCA	G-Sn-Pg
Tip rotation Angle	TRA	180-(Prn-Cm-Sn)
Nostril Angle*	NOA	NtR-NbR-Sn
Nasal Tip Angle	NTA	Stb-Prn-Sn
Ratio		
Nasal width Index	NWI	NBW/FW2
Nasal length Index	NLI	NL/FL
Dorsum Index-1	DI-1	SSn/NL
Dorsum Index-2	DI-2	SSn/Stm
Nasolabial Index	NOI	SSt/SMe
Dorsal bridge Index	DBI	DBW/EnD
Tip Aspect ratio	TAR	TW/TL
Nostril Aspect ratio*	NAR	NLA/NSA
Nasal Septum Index*	NSI	NSL/NSL+PRC

** Both sides*

Face Width

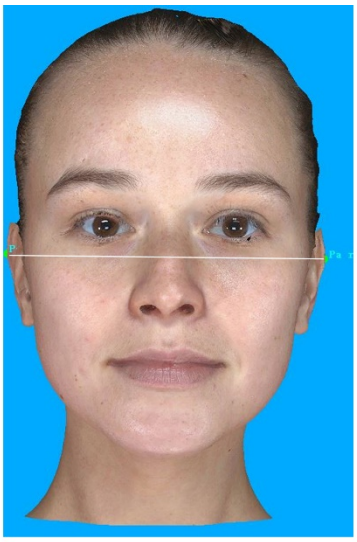

Face Width2

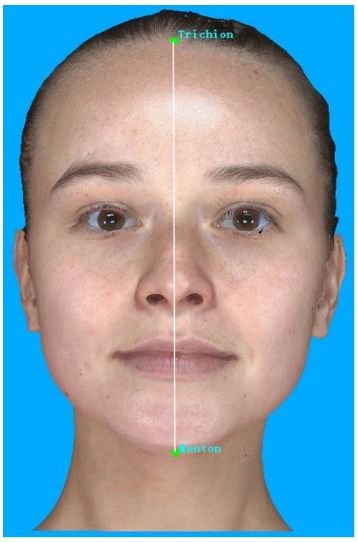

Face Length

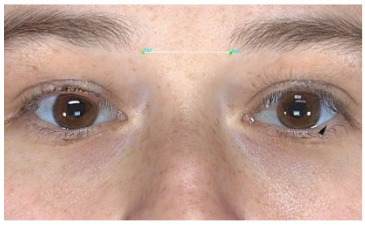

Nasal root width

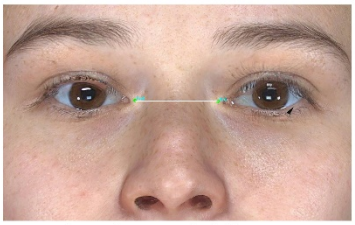

Inner intercanthal distance

SSn

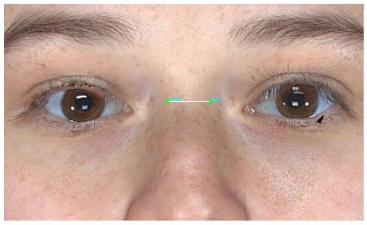

Dorsal bridge width

Nasal length

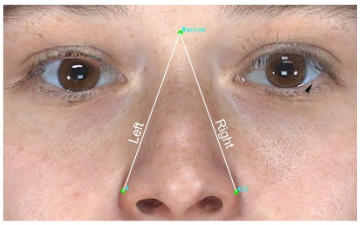

Nasion-Alare

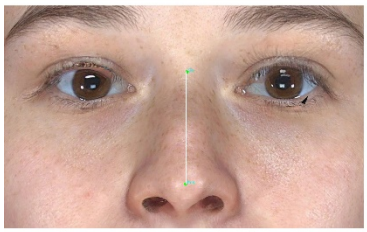

Dorsum length

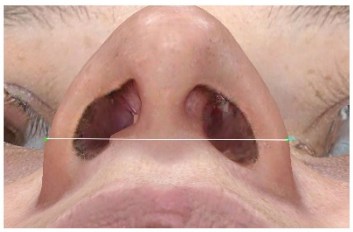

Alar base width

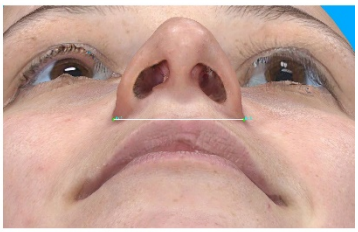

Nasal base width

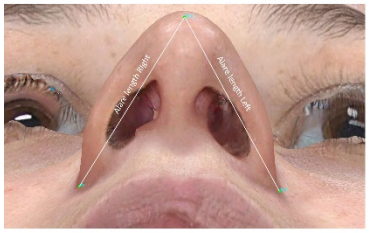

Alare Length

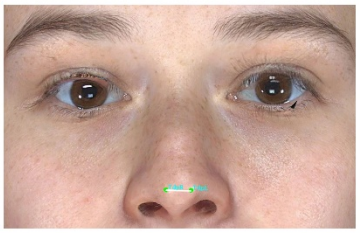

Tip Width

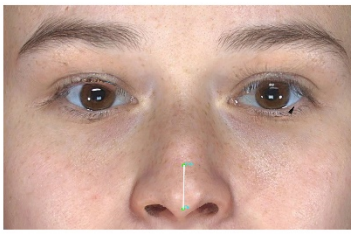

Tip Length

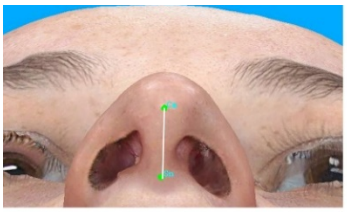

Nasal Septum length

PRC

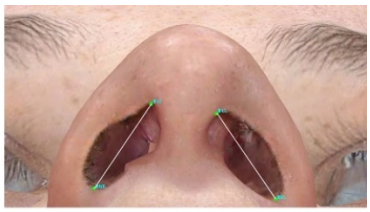

Nostril long Axis length

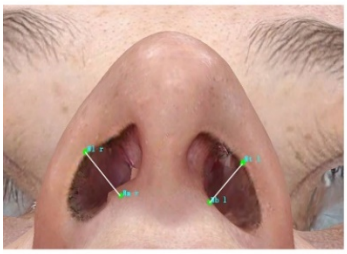

Nostril short Axis length

SSt

StM

SMe

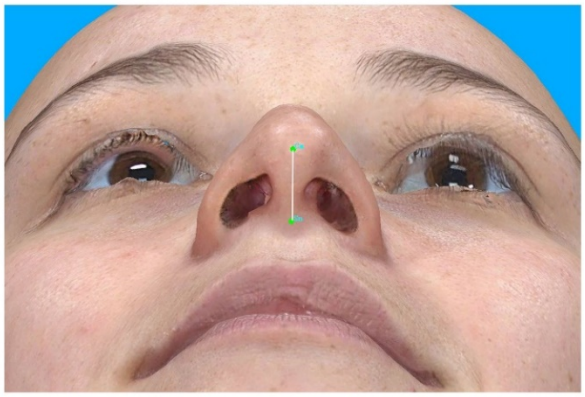

CSn

Figure 8. The measurements of projective linear distances

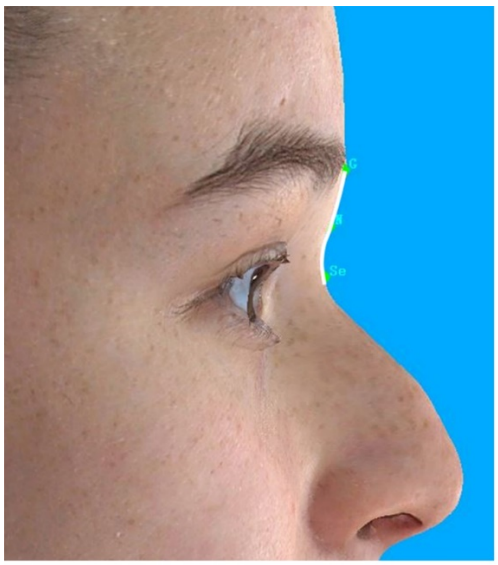

GNS

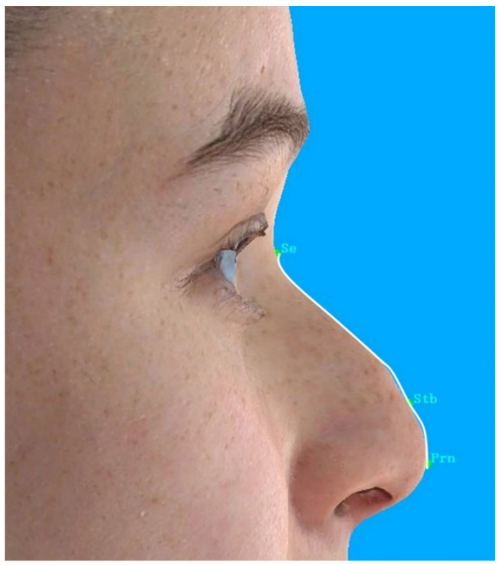

DSL

Figure 9. The measurements of surface linear distances

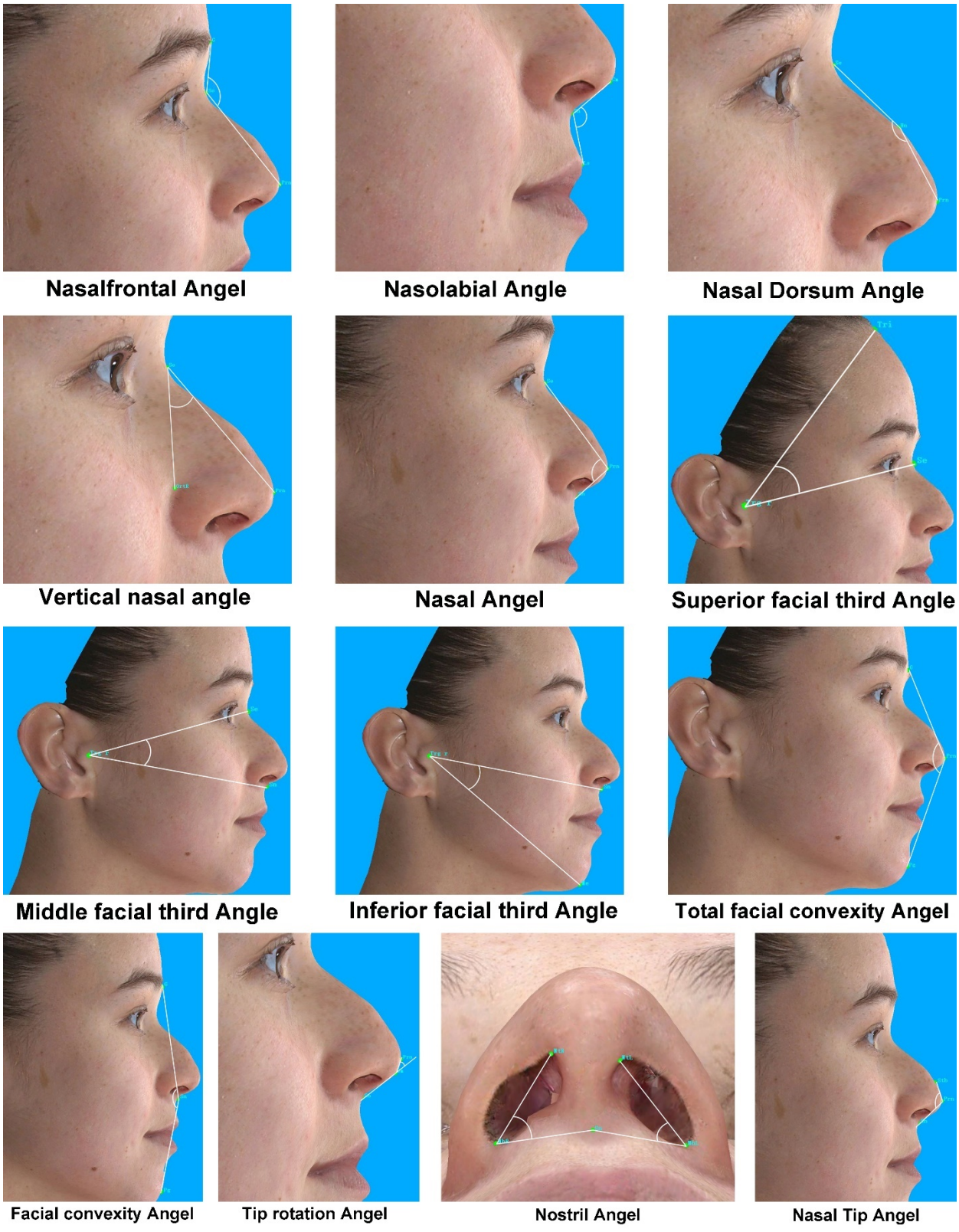

Figure 10. The measurements of Angles

3.6 The Reliability of the Landmarks

For intra-rater reliability, we compared the measurement results of two sessions by each rater. For inter-rater reliability, we compared the measurement results between rater pairs. Subsequently, the rater registered two captures, then selected all the landmarks on the capture 1, and projected them to correspondent capture 2. According to the measurement results of the two images, the intra-method reliability was calculated.

We calculated five statistic indices to evaluate the intra-rater and inter-rater reliabilities **(Table 4)**. The ICC indicates high reliability when verging on one and low reliability when verging on zero. Four classes of ICC were defined according to the consensus: < 0.5, poor; 0.5 to 0.75, moderate reliability; 0.75 to 0.9, good reliability; and ≥ 0.9, excellent[66-67]. The MAD was expressed as the absolute value of the difference between the average values of each variable calculation result between two measurements. The TEM refers to the square root of measurement error variance, and the formula for its calculation was listed in **Table 4**[68]. TEM (intra) is the intra-rater TEM for the rater 1. TEM (inter) is the interrater TEM between the two raters. TEM (intra-method) is the TEM between two captures of same volunteers. Since the size of MAD and TEM is highly positively correlated with the size of the measured value, we combined REM and rTEM to compare the measurement deviation of different variables. REM offers an estimated value of the diversity relative to the size of the measurement results, and rTEM reflects the deviation. The calculation method for REM and rTEM is to divide the MAD and TEM by the grand mean of the target variable, and then multiply by 100[31]. Based on the classification criteria proposed by previous research, REM were divided into five grades: < 1%, excellent; 1 to 3.9%, very good; 4 to 6.9%, good; 7 to 9.9%, moderate; and > 10%, poor[69-70]. The excellent ranges for rTEM for intra-rater is < 1.5% and for inter-rater is < 2.0%[71].

Table 4. Summary of reliability estimates evaluated

Statistics	Equation
Intraclass correlation coefficient (ICC)	B / (B+W)
Mean absolute difference (MAD)	|X1-X2|
Relative error measurement (REM)	(MAD/X3) x 100
Technical error of measurement (TEM)	$\sqrt{(\sum D^2/2N)}$
Relative TEM (rTEM)	(TEM/X3) × 100

B, between-measurement variance. W, within measurement variance; D, difference between measurements. N, number 147 of subjects measured. X1, mean for rater 1 (session 1, or session 2 of capture 1). X2, mean for rater 2 (session 2, or 148 session 2 of capture 2); X3, grand mean.

3.7 The Reproducibility of the Landmarks

The first rater evaluated the reproducibility of all landmarks in a two-week interval for intra-rater reproducibility. Then, we compared the assessment results of two raters for inter-rater reproducibility. According to the intra-rater and inter-rater assessment results of 160 volunteers, we calculated the mean and standard deviation for each landmark. The error of the landmarks was presented as the measurement absolute difference value of each landmark on three axes. It was divided into three categories (<0.5mm, <1mm, and >1mm). Coordinates with a difference less than 0.5mm between the measured values of all samples were classified as high reproducibility; with difference between 0.5mm and 1mm were determined as medium reproducibility; with a difference of more than 1mm were considered to be poorly reproducible[72-73]. Both intra- and inter-rater evaluations assessed the reproducibility of landmarks in three planes for all samples divided into race and gender. A total of 88320 variables (46 landmarks × 160 subjects × 3 planes × 2 raters × 2 measurements) were analyzed. Based on the

absolute value difference of each landmark on the x, y, and z axes, we used the following formula to calculate the total average reproducibility difference: $= \sqrt{\frac{(\Delta X)^2+(\Delta Y)^2+(\Delta Z)^2}{3}}$, where T is total average difference, ΔX is the difference on the x axis, ΔY is the difference on the y axis and ΔZ is the difference on the z axis. Each variable was first corrected to the median for all volunteers. The Bland-Altman plots were carried out for intra- and inter-rater reproducibility assessments. For each plot, the difference between the measurements values of each landmark coordinate was calculated and generated against the average measurement value of that particular coordinate. The vertical axis of Bland-Altman plots shows the measurement differences for the selected landmarks, while the horizontal axis shows the average of the measurements. The zero line refers to the subject with zero measurement variance (highest reproducibility). The two dashed lines above and below the zero line indicate the subject with the highest difference between the two measurement sessions.

3.8 Statistical Analysis

Statistical analyses were performed using SPSS Statistics 23.00 (IBM, Armonk, NY, USA). Data normality was tested using the Kolmogorov-Smirnov test for all measurements, and all the results are in accordance with normal distribution. GraphPad Prism 8 was used to depict the figures. The difference was considered statistically significant at a probability level of ≤ 0.05 to guide conclusions.

4 Results

4.1 Reliability

4.1.1 Overall Reliability

Study participants were between 20 and 50 years of age. Among the volunteers we recruited, there was no statistical difference between the ages of male (31.36±4.68 years old) and female (29.50±3.97 years old). **Table 5** shows the descriptive statistics (mean ***μ*** and standard error ***SD***) for each variable of intra-rater and inter-rater as well as the corresponding significance (*P)* value. All measurements were divided into four types (straight-line distance, surface distance, angle, and ratio). The reliability of intra-rater, inter-rater, and intra-method are shown in **Table 6** to **8.**

Table 5. Overview of the reliability results of two raters

Variable	Rater 1				*P* value	Rater 2		*P* value
	Measurement session1		Measurement session2			Measurement		
	μ	*SD*	*μ*	*SD*		*μ*	*SD*	
NFRA	144.053	6.517	144.097	6.406	0.756	144.471	6.182	0.087
NLA	121.435	9.537	121.725	9.554	0.285	120.587	9.911	0.113
NDA	174.687	3.016	174.87	3.191	0.452	174.109	3.404	<0.001
VNAr	44.146	3.499	44.022	3.276	0.504	43.075	4.412	0.269
VNAl	43.244	3.422	43.152	3.258	0.668	41.798	4.424	0.344
NA	97.425	4.492	97.371	4.597	0.79	98.226	4.546	<0.001
SFAr	29.79	3.995	29.776	3.897	0.913	29.42	3.942	0.114
SFAl	30.046	3.865	29.877	3.892	0.14	29.727	3.908	0.325
MFAr	23.761	1.55	23.886	1.409	0.281	24.189	1.494	0.001
MFAl	24.111	1.538	24.162	1.506	0.557	24.67	1.546	<0.001
IFAr	28.857	2.49	28.957	2.486	0.507	28.56	2.524	0.06
IFAl	29.087	2.356	29.139	2.485	0.695	28.754	2.471	0.132
TFCA	136.938	5.225	136.904	5.147	0.684	137.71	5.289	<0.001
FCA	163.636	5.392	163.648	5.609	0.946	165.113	5.195	<0.001

TRA	36.914	7.479	36.779	6.862	0.806	36.368	6.717	0.39
NOAr	49.857	7.962	49.736	6.837	0.855	50.391	6.635	0.174
NOAl	47.444	7.748	47.238	8.223	0.79	47.888	7.601	0.298
NTA	79.58	8.018	79.322	7.947	0.581	79.235	7.764	0.621
FW	117.954	8.291	118.712	5.811	0.623	120.123	6.068	<0.001
FW2	171.488	12.242	171.364	12.7	0.585	171.34	12.729	0.473
FL	186.325	10.136	186.343	10.069	0.932	186.698	9.752	0.288
NRW	26.158	4.748	26.145	4.392	0.94	25.457	4.559	0.005
EnD	29.34	2.328	29.239	2.19	0.474	29.287	2.501	0.989
SSn	51.673	3.712	51.829	3.776	0.318	52.91	3.937	<0.001
DBW	14.766	2.445	14.48	2.61	0.082	13.717	2.657	<0.001
NL	66.652	4.235	66.687	4.364	0.854	68.683	4.705	<0.001
NAAr	52.381	3.861	52.439	3.877	0.708	53.287	3.518	0.002
NAAl	52.247	3.871	52.42	3.762	0.32	53.218	3.902	0.004
DL	45.663	4.051	45.88	4.089	0.134	46.835	3.843	0.054
ABW	30.439	3.473	30.424	3.49	0.908	31.042	3.236	<0.001
NBW	30.666	3.004	30.512	3.053	0.254	30.439	3.771	0.588
ALLr	31.816	2.743	31.623	3.018	0.212	31.791	2.965	0.691
ALLl	32.21	2.671	31.875	3.004	0.042	31.895	2.971	0.416
TW	10.108	1.497	9.919	1.465	0.093	10.288	1.638	0.071
TL	10.894	1.554	10.755	1.489	0.177	10.963	1.917	0.429
NSL	15.06	1.928	15.125	1.885	0.644	15.755	2.172	<0.001
PRC	6.31	1.022	6.219	0.91	0.287	6.198	0.863	0.33
NLAr	14.807	1.949	14.798	1.954	0.907	15.122	2.77	0.157
NLAl	14.958	2.104	15.036	2.17	0.385	15.202	2.195	0.012
NSAr	6.616	1.203	6.693	1.185	0.072	7.175	1.228	<0.001
NSAl	6.278	1.187	6.275	1.083	0.951	6.594	1.144	<0.001
SSt	21.64	2.222	21.711	2.189	0.645	20.697	2.419	<0.001
SMe	69.163	5.508	69.235	5.523	0.779	67.826	5.068	0.002
StM	47.768	4.365	47.762	4.411	0.979	47.37	4.171	0.236
CSn	15.06	1.928	15.125	1.885	0.644	15.942	2.833	<0.001
GNS	15.505	2.591	15.405	2.334	0.227	15.901	2.693	0.03
DSL	46.538	4.251	46.63	4.175	0.128	46.285	3.121	0.073
NWl	0.18	0.017	0.179	0.017	0.596	0.178	0.02	0.281
NLl	0.358	0.022	0.358	0.023	0.882	0.367	0.023	<0.001
Dl1	0.776	0.033	0.777	0.031	0.466	0.772	0.031	0.302
Dl2	1.089	0.107	1.092	0.112	0.493	1.108	0.105	0.003
NOl	0.313	0.024	0.314	0.023	0.673	0.31	0.025	0.084
DBl	0.504	0.079	0.496	0.084	0.215	0.493	0.081	0.172
TAR	0.939	0.147	0.931	0.136	0.554	0.943	0.13	0.048
NARr	2.264	0.366	2.258	0.38	0.615	2.195	0.313	0.108
NARl	2.424	0.444	2.437	0.429	0.398	2.378	0.437	0.001
NSl	0.704	0.04	0.708	0.038	0.265	0.72	0.044	0.001

4.1.2 Intra-rater Reliability of Landmarks

Overall, all measurements displayed a good reliability with an ICC above 0.75 **(Table 1, Attachment)**. Of these, 41 measurements showed excellent reliability with an ICC larger than or equal to 0.9. The highest ICC was found in the TFCA with 0.995 and the lowest in the NOAI with 0.77. The MAD were less than 0.3mm for most straight-line distances, although magnitudes reached 0.758mm for face width and 0.335mm for alare length left. The MAD of surface distance, GNS, and DSL were 0.1mm and 0.216mm respectively. The MAD of all angles were smaller than 0.3 degree, and MAD are less than 0.01 for ratio measurements except for NAR left (0.013). Fifty measurements of estimates for the relative error magnitude were less than 1%. Seven measurements had a relative error magnitude between 1% and 2%. The DBW showed the highest relative error magnitude with 1.958%. Furthermore, all rTEM estimates were in very good reliability **(Figure 11)**.

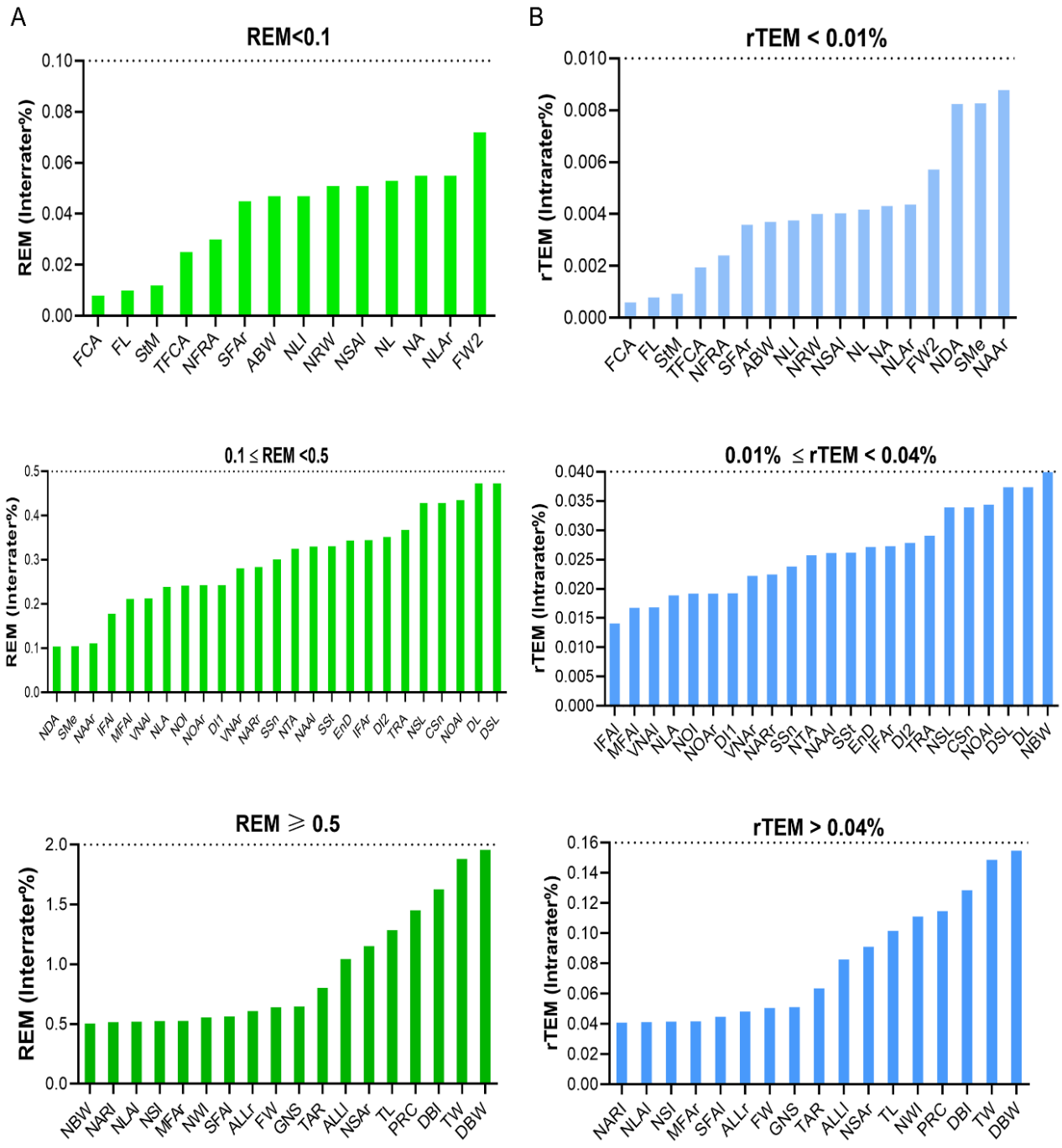

Figure 11. Intra-rater REM and rTEM across all nasal measurements on 3D images. (0.001% as one unit)

4.1.3 Inter-rater Reliability of Landmarks

The ICC values of 23 measurements were excellent with an ICC value larger than or equal to 0.9. Except for the TL with 0.732, the remaining measurements showed a good reliability with an ICC above 0.75. Among them, 28 measurements showed an ICC of 0.80 to 0.89. Lowest ICC between 0.75 and 0.79 were found in TW, NLA left, IFAL, NDA, and CSn **(Table 2, Attachment)**.

The MAD were less than or closely around 1mm for most straight-line distances. Only four measurements showed more than 1mm deviation. The highest deviation was found in the NL with 2.013mm. The MAD of surface distance were 0.803mm and 0.513mm for GNS and DSL respectively. MAD were less than 1 degree for most angle variables, although they were larger for VNA right and VNA left. MAD was 1.47 degree for FCA. The relative error magnitude estimates for eighteen measurements were excellent with less than 1% REM. 32 measurements had a relative error magnitude between 1 and 3.9% (very good), six measurements had a relative error magnitude between 4 and 7% (good), and the columella width had a relative error magnitude of 7.522% (moderate). The rTEM were less than 0.1% for most measurements; however, estimates were greater for tip length **(Figure 12).**

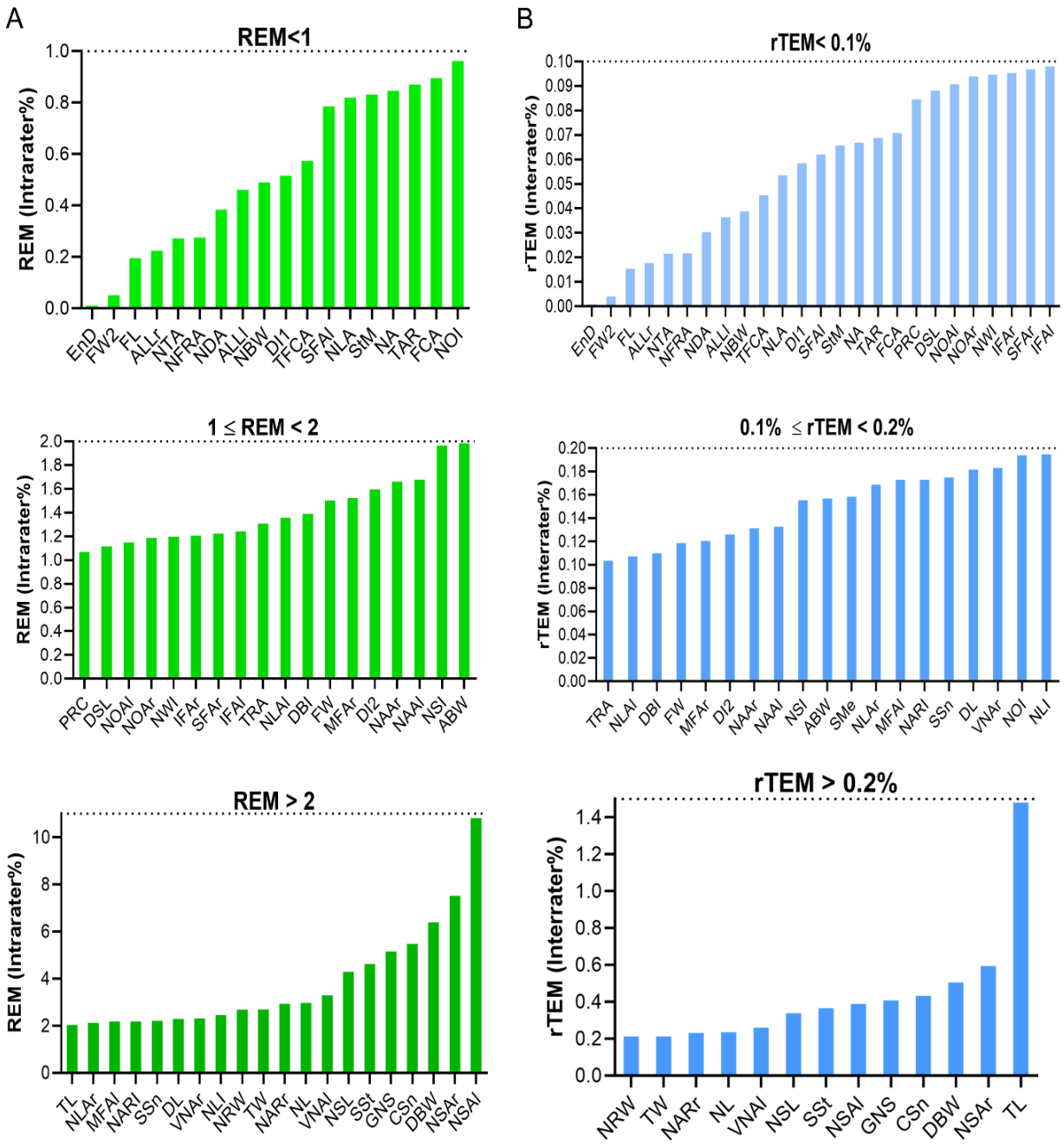

Figure 12. Inter-rater REM and rTEM across all nasal measurements on 3D images

4.1.4 Intra-method Reliability with VECTRA XT Imaging System

ICC estimates were excellent across all measurements: larger than or equal to 0.95 for 56 of the 57 measurements. Smallest ICC was found in the NOAI with 0.948. The MAD were less than 0.3mm for most straight-line distances except for the FW with 0.758. The MAD of surface distance, GNS and DSL were 0.05mm and 0.379 mm, respectively. Similar to intra-rater reliability, 18 of 19 angle variable's MAD were smaller than 0.2 degree, and the nasofrontal angle had the largest value of 0.598. For the ratio variables, MAD were all less than 0.01, among them, NARI has the largest value of 0.006 **(Table 3, Attachment)**.

All estimates for REM were less than 1%. Eighteen measurements had a REM smaller than 0.1%, 16 measurements had a relative error magnitude between 0.1 and 0.2%, 23 measurements had a relative error magnitude larger than 0.2%, and the largest relative error magnitude for DBW is 0.984%. The rTEM was less than 0.1% for all measurements **(Figure 13)**. Seventeen variables were smaller than 0.005%, 21 variables are between 0.01 and 0.02%, and 19 measurements were higher than 0.02%.

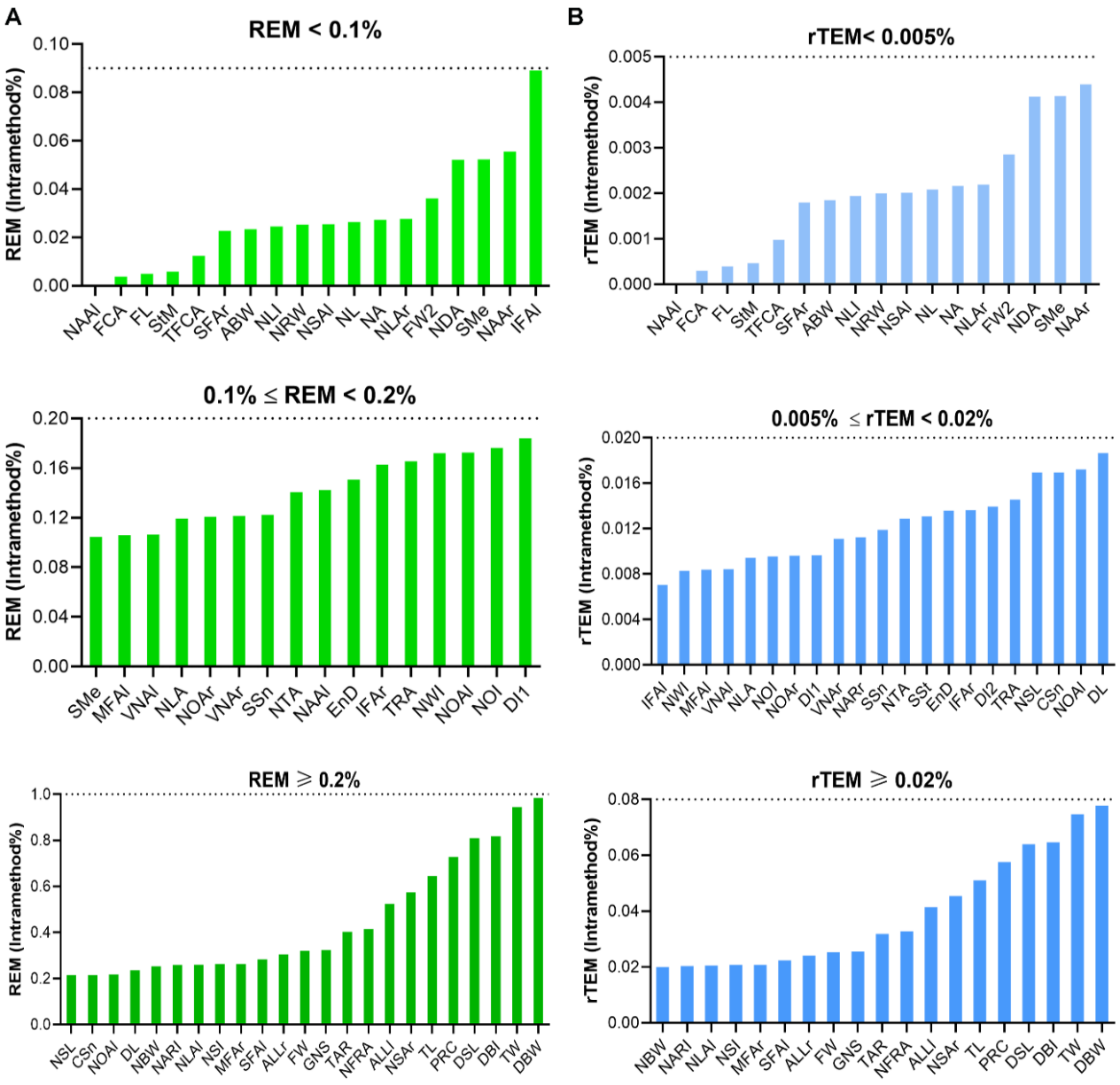

Figure 13. Inter-method REM and rTEM across all nasal measurements on 3D images.

4.2 Reproducibility

4.2.1 Overall Reproducibility

Table 6 shows the overall results of reproducibility of coordinates gained from intra- and inter-rater results in 160 volunteers. Besides, we also display the results separately according to race and gender.

Generally, reproducibility was less than 1mm in most assessment (intra-rater 87% and inter-rater 73.2% overall). In Caucasian subgroups, the intra-rater was 83.4% and inter-rater was 71.1%; in Asian subgroups, the intra-rater was 79.7% and the inter-rater was 72.5%. In females, the intra-rater was 79.7% and inter-rater was 69.6%; in males, the intra-rater was 82.6% and the inter-rater was 73.2%. The highest reproducibility (<0.5mm) coordinates made up 45% (intra-rater) and 31.2% (inter-rater) in 160 samples. The worst reproducibility (>1mm) coordinates accounted for 13% (intra-rater) and 26.8% (inter-rater).

After all samples were grouped according to gender and race, the error results of all landmarks on the x-, y-, and z-axes were shown in **Tables 4** and **5 in attachment** respectively. Additionally, we calculated the total error based on the results on each axis for every landmark. The landmarks were ranked from most reproducible to least reproducible for both intra- and inter-rater assessments. Compared to the intra-rater assessment, we noticed that the correspondent inter-rater results showed a poorer reproducibility.

Table 6. Overall Reproducibility of identified landmarks

Method of assessment	Intra-rater						Inter-rater					
Total	n=160						n=160					
Reproducibility level (mm)	<0.5		0.05≤d<1		d≥1		<0.5		0.05≤d<1		d≥1	
Number of coordinates	62		58		18		43		58		37	
Percentage (%)	45		42		13		31.2		42		26.8	
Race	Caucasian (n=80)			Asian (n=80)			Caucasian (n=80)			Asian (n=80)		
Reproducibility level (mm)	<0.5	0.05≤d<1	d≥1	<0.5	0.05≤d<1	d≥1	<0.5	0.05≤d<1	d≥1	<0.5	0.05≤d<1	d≥1
Number of coordinates	63	52	23	51	59	28	42	56	40	43	57	38
Percentage (%)	45.7	37.7	16.6	37	42.7	20.3	23.2	40.6	28.9	31.2	41.3	27.5
Gender	Female (n=80)			Male (n=80)			Female (n=80)			Male (n=80)		
Reproducibility level (mm)	<0.5	0.05≤d<1	d≥1	<0.5	0.05≤d<1	d≥1	<0.5	0.05≤d<1	d≥1	<0.5	0.05≤d<1	d≥1
Number of coordinates	58	52	28	62	52	24	41	55	42	42	59	37
Percentage (%)	42	37.7	20.3	44.9	37.7	17.4	29.7	39.9	30.4	30.4	42.8	26.8

Total number of coordinates = 138

4.2.2 The Landmarks' Reproducibility in Caucasian and Asian Participants

The accuracy of landmarks in the Caucasian group ranged from 0.17 to 0.94 mm (intra-rater) and 0.20 to 1.38 mm (inter-rater) in the nose area, 0.44 to 0.61 mm (intra-rater) and 0.49 to 0.95 mm (inter-rater) in the eye area, 0.44 to 1.47 mm (intra-rater) and 0.52 to 1.75 mm (inter-rater) in the mouth area, 0.72 to 1.07 mm (intra-rater) and 1.19 to 1.63

mm (inter-rater) in the ear area, and 1.52 to 1.79 mm (intra-rater) and 1.23 to 2.04 mm (inter-rater) in other areas.

The accuracy of landmarks in the Asian group ranged from 0.20 to 1.38 mm (intra-rater) and 0.25 to 1.13mm (inter-rater) in the nose area, 0.30 to 0.62 mm (intra-rater) and 0.54 to 0.85 mm (inter-rater) in the eye area, 0.47 to 1.52 mm (intra-rater) and 0.67 to 1.73 mm (inter-rater) in the mouth area, 0.86 to 0.97 mm (intra-rater) and 1.05 to 1.40 mm (inter-rater) in the ear area, and 1.23 to 2.04 mm (intra-rater) and 1.43 to 2.21 mm (inter-rater) in other areas.

The main reproducibility difference of landmarks between Caucasian and Asian focused on nose tip, alare, and nostril area, which included Sn, Cc, Cm, Al right, Al left, Ac right, Nm of both sides and Stb point. Several landmarks show poor reproducibility in both Caucasians and Asians, namely Tri, Zy right and Zy left. The landmark with most significant intra- and inter-group difference was Zy left among Caucasians with 0.8 mm and Pa right among Asians with 0.43 mm. Moreover, the measurement difference between intra-group and inter-group assessment of landmarks in the Asian group were generally smaller than in the Caucasian group. The most reproducible and least reproducible landmarks among Asians were consistent with those among Caucasians **(Table 7 and Table 4 in attachment).**

Table 7. Rankings of facial soft tissue landmarks in Caucasian and Asian in respect to their reproducibility in the three spatial planes

Race	Caucasian (n=80)					Asian (n=80)				
Area	Landmarks	Intra-rater		Inter-rater		Landmarks	Intra-rater		Inter-rater	
		Mean	SD	Mean	SD		Mean	SD	Mean	SD

Nose	Nl l	0.17	0.14	0.34	0.23	Nl l	0.20	0.15	0.25	0.22
	Nl r	0.17	0.12	0.43	0.45	Nl r	0.24	0.21	0.28	0.26
	Nb l	0.20	0.14	0.48	0.49	Nb r	0.25	0.17	0.30	0.23
	Nb r	0.21	0.26	0.48	0.15	Nb l	0.27	0.30	0.38	0.28
	Nt r	0.22	0.16	0.51	0.46	Nt r	0.30	0.27	0.39	0.36
	Nt l	0.23	0.15	0.54	0.27	Nt l	0.43	0.36	0.49	0.34
	Nm l	0.25	0.19	0.55	0.33	Cc	0.43	0.38	0.54	0.42
	Nm r	0.26	0.19	0.55	0.49	Cm	0.43	0.28	0.60	0.47
	G	0.31	0.21	0.61	0.38	G	0.44	0.38	0.63	0.48
	Prn	0.31	0.21	0.71	0.55	Prn	0.44	0.32	0.63	0.52
	Cm	0.35	0.24	0.72	0.53	Al l	0.45	0.57	0.65	0.53
	Stb	0.39	0.29	0.79	0.56	Al r	0.58	0.46	0.71	0.44
	TDP r	0.44	0.40	0.84	0.65	TDP r	0.59	0.51	0.71	0.57
	TDP l	0.44	0.39	0.85	0.62	TDP l	0.65	0.55	0.74	0.69
	Se	0.48	0.40	0.88	0.75	Se	0.68	0.63	0.76	0.58
	Cc	0.54	0.39	0.92	0.55	Nm r	0.69	0.50	0.77	0.63
	Ac l	0.64	0.47	0.93	0.72	Nm l	0.71	0.60	0.78	0.57
	Holn	0.67	0.47	1.00	0.69	Holn	0.78	0.70	0.98	0.73
	Ac r	0.68	0.50	1.01	0.75	Ac r	0.86	0.67	0.99	0.71
	Se'r	0.69	0.54	1.03	0.72	Se'r	0.93	0.51	1.00	0.82
	Se'l	0.72	0.69	1.06	0.74	Se'l	0.94	0.75	1.07	0.94
	N	0.73	0.44	1.07	0.50	N	0.95	0.60	1.08	0.86
	Al l	0.75	0.61	1.09	0.68	Ac l	0.95	0.46	1.09	0.51
	Al r	0.75	0.55	1.11	0.64	Stb	1.04	0.62	1.10	0.71
	Sn	0.83	0.57	1.15	0.58	Sn	1.04	0.86	1.11	0.83
	Ort l	0.90	0.60	1.18	0.73	Ort l	1.04	0.97	1.13	0.78
	Ort r	0.94	0.66	1.20	0.87	Ort r	1.11	0.69	1.13	0.74
Eye	En r	0.44	0.31	0.49	0.35	En r	0.30	0.22	0.54	0.41
	En l	0.49	0.34	0.65	0.51	En l	0.38	0.30	0.67	0.53
	Em r	0.54	0.30	0.66	0.30	Em r	0.61	0.46	0.77	0.47
	Em l	0.61	0.55	0.95	0.72	Em l	0.62	0.57	0.85	0.55
Mouth	Sto	0.43	0.27	0.52	0.43	Sto	0.47	0.27	0.64	0.57
	Li	0.43	0.36	0.58	0.32	Li	0.49	0.51	0.67	0.43
	Ls	0.44	0.33	0.60	0.36	Ls	0.61	0.47	0.68	0.52
	Sm	0.60	0.45	0.66	0.61	Sm	0.64	0.47	0.81	0.52
	Sl	0.75	0.46	0.85	0.50	Sl	0.86	0.64	0.95	0.48

	Pg	0.98	0.72	1.45	0.65	Pg	1.21	1.03	1.31	0.78
	Me	1.11	0.91	1.54	1.25	Me	1.50	1.14	1.63	1.03
	C	1.47	0.84	1.75	1.22	C	1.52	0.94	1.73	0.69
Ear	Trg l	0.72	0.54	1.19	1.19	Trg l	0.86	0.73	1.05	0.74
	Trg r	0.87	0.68	1.29	0.67	Trg r	0.88	0.76	1.22	0.88
	Pa l	0.90	0.63	1.59	0.65	Pa l	0.89	0.55	1.29	0.92
	Pa r	1.07	0.69	1.63	0.68	Pa r	0.97	0.89	1.40	0.90
Others	Tri	1.52	1.10	1.94	1.05	Tri	1.23	0.95	1.43	0.99
	Zy r	1.62	0.97	2.00	1.02	Zy r	2.01	1.08	2.12	1.30
	Zy l	1.79	1.38	2.59	1.19	Zy l	2.04	1.25	2.21	1.12

4.2.3 The Landmarks' Reproducibility in Female and Male Subgroups

The accuracy for landmarks in the female subgroup ranged from 0.24 to 1.55 mm (intra-rater) and 0.32 to 1.88 mm (inter-rater) in the nose area, 0.31 to 0.53 mm (intra-rater) and 0.45 to 0.76 mm (inter-rater) in the eye area, 0.40 to 1.33 mm (intra-rater) and 0.53 to 1.83 mm (inter-rater) in the mouth area, 0.79 to 1.22 mm (intra-rater) and 1.40 to 1.99 mm (inter-rater) in the ear area and 1.19 to 1.97 mm (intra-rater) and 1.17 to 2.25 mm (inter-rater) in other areas.

The accuracy for landmarks in the male subgroup ranged from 0.21 to 1.45 mm (intra-rater) and 0.31 to 1.65 mm (inter-rater) in the nose area, 0.38 to 0.68 mm (intra-rater) and 0.49 to 0.85mm (inter-rater) in the eye area, 0.41 to 1.08 mm (intra-rater) and 0.50 to 1.57 mm (inter-rater) in the mouth area, 0.83 to 1.14 mm (intra-rater) and 1.20 to 2.06 mm (inter-rater) in the ear area and 1.28 to 1.45 mm (intra-rater) and 1.03 to 2.43 mm (inter-rater) in other areas.

We didn't notice a significant difference in ranking of landmark reproducibility between genders in general, except for Sellion right, Nostril base point left and right. The landmarks, concentrating on nose and mouth, were observed to have higher reproducibility in males compared to females in intra-rater, while the landmarks in eye area were noticed to have poorer reproducibility in males, and the deviations between intra- and inter-rater in males were smaller than in females. In both female and male groups, the pronasale (prn) was the most reproducible landmark and the landmarks Zygion left was the least reproducible **(Table 8 and Table 5 in attachment)**.

Table 8. Ranking of facial soft tissue landmarks in females and males in respect to their reproducibility in the three spatial planes

Gender	Female (n=80)					Male (n=80)				
Area	Landmarks	Intra-rater		Inter-rater		Landmarks	Intra-rater		Inter-rater	
		Mean	SD	Mean	SD		Mean	SD	Mean	SD
Nose	Prn	0.24	0.22	0.32	0.21	Prn	0.21	0.19	0.31	0.19
	Cm	0.25	0.21	0.34	0.27	Cm	0.23	0.20	0.32	0.14
	Holn	0.25	0.16	0.35	0.26	Holn	0.23	0.17	0.33	0.14
	TDP r	0.30	0.22	0.35	0.25	TDP r	0.27	0.19	0.36	0.20
	TDP l	0.34	0.91	0.56	0.48	TDP l	0.30	0.53	0.52	0.43
	Se	0.38	0.38	0.59	0.19	Se	0.31	0.32	0.52	0.36
	G	0.39	0.30	0.70	0.55	G	0.32	0.24	0.57	0.45
	Ac l	0.38	0.93	0.77	0.52	Ac l	0.36	0.45	0.59	0.53
	Ac r	0.42	0.23	0.77	0.52	Ac r	0.38	0.32	0.72	0.62
	Nt l	0.43	0.33	0.79	0.57	Nt l	0.39	0.22	0.72	0.47
	Nt r	0.46	0.40	0.83	0.55	Nt r	0.40	0.23	0.75	0.48
	Nl l	0.47	0.43	0.84	0.59	Nl l	0.46	0.46	0.89	0.64
	Nl r	0.54	0.47	0.93	0.75	Nl r	0.49	0.53	0.95	0.84
	Ort l	0.57	0.44	0.94	0.62	Ort l	0.52	0.30	1.03	0.94
	Ort r	0.59	0.30	0.95	0.61	Ort r	0.53	0.36	1.04	0.74
	Cc	0.65	0.41	0.95	0.75	Cc	0.62	0.54	1.12	1.03
	Sn	0.66	0.58	0.85	0.56	Sn	0.64	0.57	0.98	0.56
	Se'l	0.66	0.55	1.04	0.64	Se'l	0.65	0.66	1.16	0.91
	Se'r	0.71	0.57	1.08	0.65	Nb l	0.73	0.49	1.20	0.49
	Nb l	0.73	0.80	1.13	0.63	Nb r	0.73	0.61	1.25	0.86
	Nb r	0.75	0.65	1.21	1.01	Se'r	0.75	0.51	1.34	0.99

	Nm l	0.80	0.56	1.30	0.48	Nm l	0.79	0.57	1.35	1.00
	Nm r	0.84	0.54	1.30	0.83	Nm r	0.80	0.73	1.42	0.75
	Al r	0.85	0.56	1.57	1.02	Al r	0.85	0.62	1.50	1.12
	Al l	0.86	0.80	1.61	1.03	Al l	0.86	0.54	1.51	1.01
	N	0.90	0.60	1.52	0.69	N	0.99	0.84	1.35	0.89
	Stb	1.55	1.01	1.88	0.91	Stb	1.45	0.92	1.65	0.76
Eye	Em l	0.31	0.26	0.45	0.35	Em l	0.38	0.29	0.49	0.36
	Em r	0.39	0.36	0.54	0.35	Em r	0.43	0.32	0.56	0.53
	En r	0.48	0.40	0.71	0.60	En r	0.67	0.50	0.79	0.82
	En l	0.53	0.44	0.76	0.67	En l	0.68	0.55	0.85	0.48
Mouth	Ls	0.43	0.36	0.53	0.42	Ls	0.41	0.29	0.50	0.70
	Li	0.52	0.48	0.62	0.32	Li	0.44	0.28	0.52	0.45
	Sto	0.59	0.46	0.68	0.50	Sto	0.45	0.40	0.54	0.27
	Me	0.60	0.55	0.82	0.59	Me	0.50	0.45	0.68	0.49
	Sl	0.72	0.60	1.04	0.81	Sl	0.70	0.54	0.99	0.58
	Pg	0.73	0.41	1.09	1.19	Pg	0.70	0.36	1.04	0.75
	Sm	1.13	1.01	1.51	1.04	Sm	1.02	0.71	1.36	0.73
	C	1.33	0.83	1.83	1.17	C	1.08	0.82	1.57	0.99
Ear	Pa l	0.79	0.52	1.40	1.07	Pa l	0.78	0.64	1.12	0.66
	Pa r	0.87	0.71	1.65	0.95	Pa r	0.84	0.65	1.13	0.66
	Trg r	1.04	0.63	1.42	0.62	Trg r	0.87	0.66	1.15	0.68
	Trg l	1.22	0.68	1.99	0.93	Trg l	1.14	0.97	1.45	0.91
Others	Tri	1.53	1.07	1.64	0.95	Tri	1.50	0.93	1.58	0.89
	Zy r	1.87	1.35	2.09	1.27	Zy r	1.64	1.06	1.92	0.99
	Zy l	1.97	1.49	2.25	1.36	Zy l	1.77	1.17	2.27	0.82

Some landmarks differed in their reproducibility levels in intra-rater and inter-rater assessments as follows: Cm and Stb were highly reproducible (<0.5 mm) in the intra-rater, and moderately (<1 mm) in the inter-rater assessment in Caucasian samples. Se right and Se left were moderately reproducible (<0.5 mm) in intra-rater and poorly (>1 mm) in inter-rater assessment in Asian samples.

4.3 The Representative Landmarks in Ethnic and Gender Subgroups

Bland-Altman plots were used to illustrate the consistency level between the values of each 3D coordinates (X, Y, and Z) for the facial landmarks. Some representative coordinates of facial landmarks are given in **Figure 14** to illustrate the high, moderate, and low levels of consistency between the measure values obtained from intra-rater assessment in ethnic subgroups. **Figure 14A** indicates that the landmark Cm has high reproducibility on X plane in Caucasians and Asians (<0.5 mm). **Figure 14B** indicates that the landmark M has moderate reproducibility on Y plane (>0.5 mm). **Figure 14C** indicates that the landmark Tri has poor reproducibility on Z plane (>1 mm). **Figure 15** exhibits the measurements obtained from the inter-rater assessment for some representative coordinates of facial landmarks in gender subgroups. **Figure 15A** indicates that the landmark Prn has high reproducibility on X plane in females and Males (<0.5 mm). **Figure 15B** indicates that the landmark N has moderate reproducibility on Y plane (> 0.5 mm). **Figure 15C** indicates that the landmark Stb point has poor reproducibility on Z plane (>1 mm).

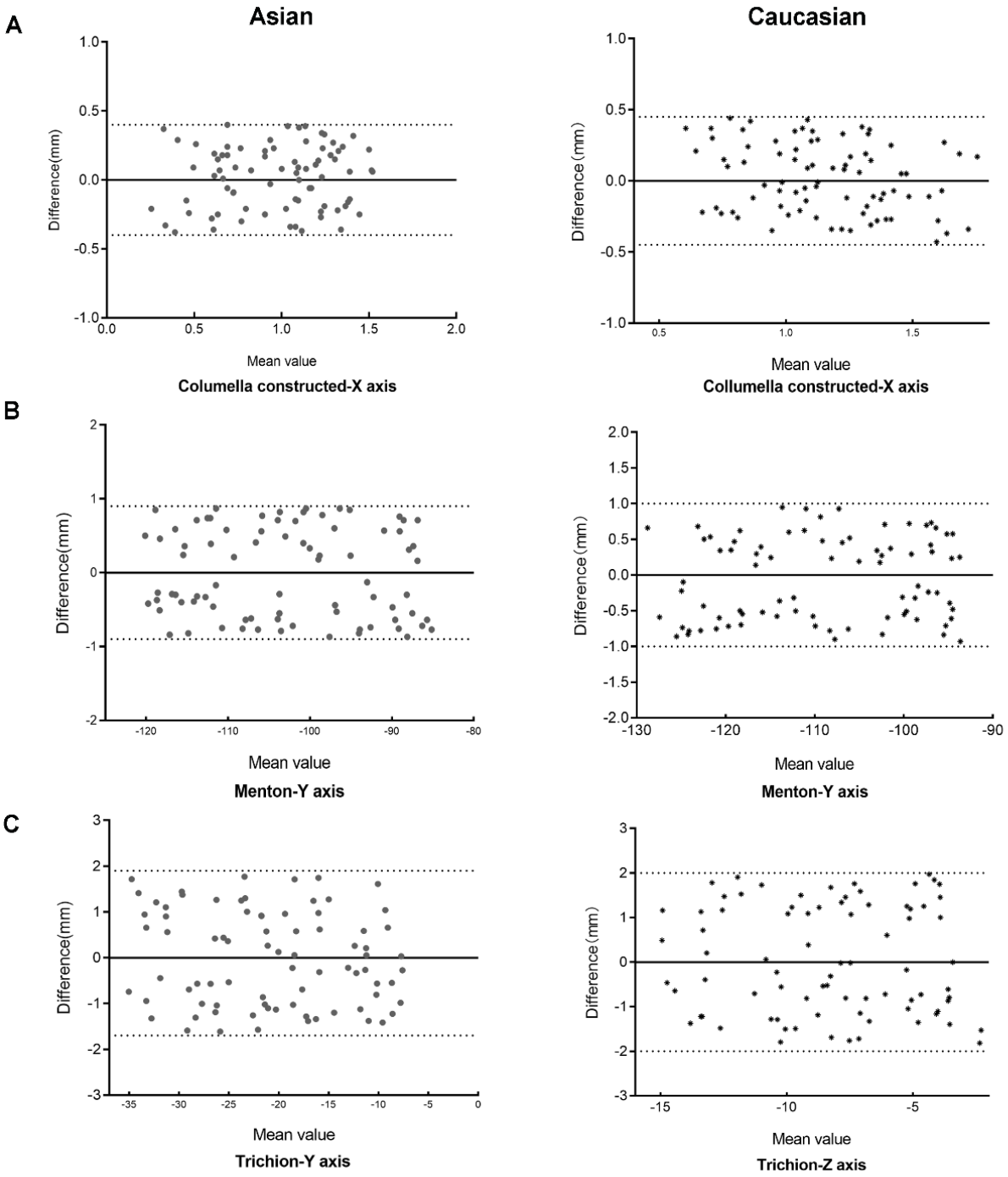

Figure 14. Reproducibility of representative landmarks identification between Caucasian and Asian (intra-rater).

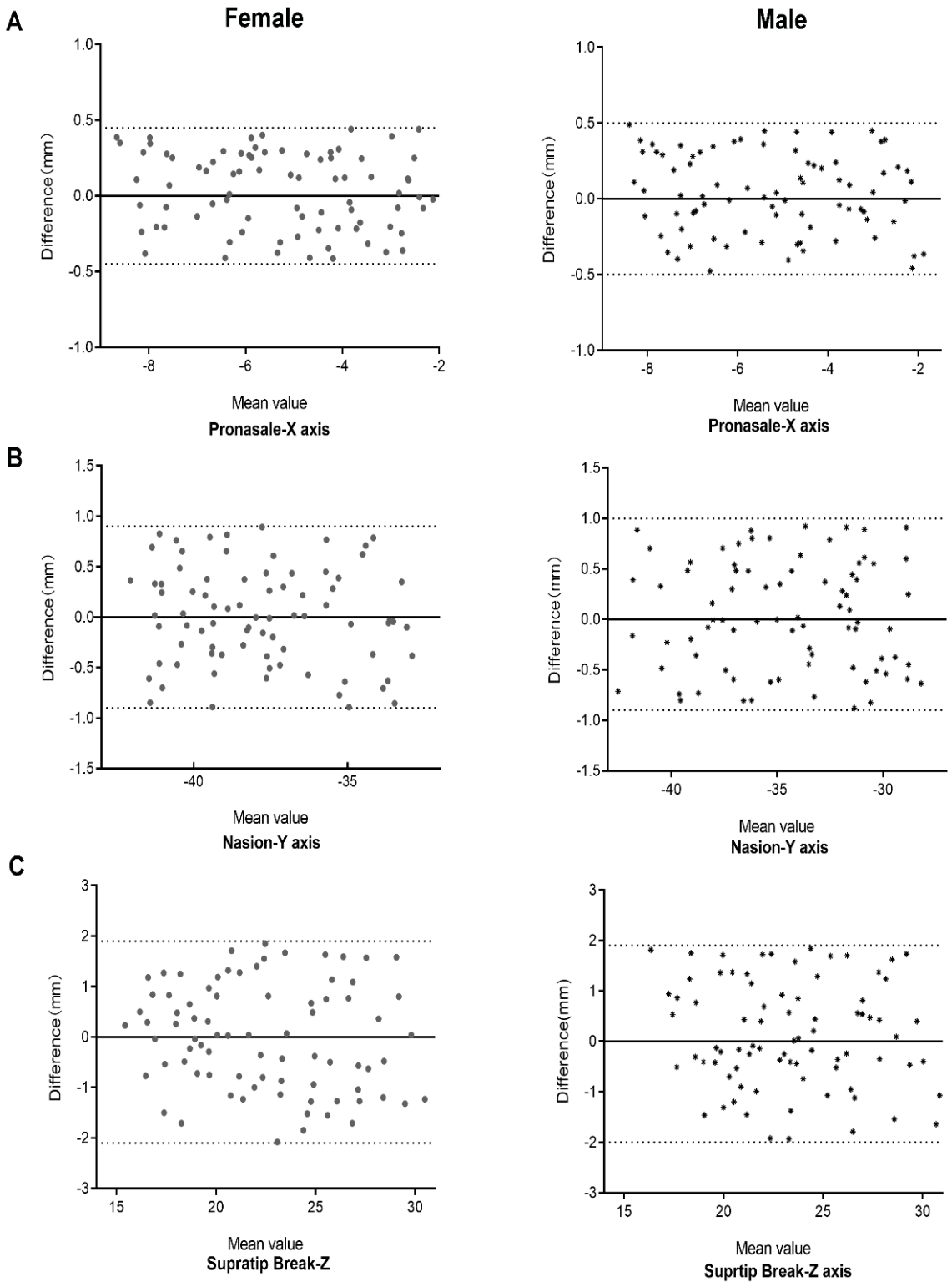

Figure 15. Reproducibility of representative landmarks identification between Female and Male (inter-rater).

5 Discussion

5.1 Study Design

Facial soft tissue landmarks and their anthropometric measurements play an important role in the clinical practice of numerous medical disciplines, especially in reconstructive and aesthetic plastic surgery, otorhinolaryngology, and oral and maxillofacial surgery. Landmark-based cephalofacial measurements can be used in diagnostics, counselling and treatment planning, as well as objective evaluation of a therapeutic outcome. The reproducibility of facial soft tissue landmarks has been studied in detail on 2D photography and several classic facial landmarks have been validated for their utility in 3D surface imaging [59-62].

Based on the current literature, the present thesis evaluated the reliability and reproducibility of facial measurements derived by 3D stereophotogrammetry in 160 volunteers. We investigated 46 traditional and non-traditional 3D soft tissue facial landmarks resulting in 57 corresponding straight and surface distances, angular measurements, and facial ratio variables with respect to their application in quantitative analysis of perinasal morphology. These landmarks and variables fully covered the nose and perinasal surface in relationship to the face. The study group was further divided into subgroups to gain a better understanding of differences in 3D landmark-based measurement.

5.2 Study Results

The overall mean values of the variables ranged from 6.264 to 186.334 mm in distance measurements, 23.824 to 174.779 degree in angle measurements, and 0.179 to 2.437 in ratios, which embraces a wide range of measurement pairs. A very high level of agreement was found for the intra-rater reliability with overall low mean differences. The highest MAD were 0.758 mm for linear measurements, 0.290 degree for angular measurements, and 0.013 for facial indices. In contrast, inter-rater reliability mean differences ranged from 0.003 to 2.013 mm in linear measurements, 0.216 to 1.471 degree for angular measurements and 0.002 to 0.065 in facial ratios.

Interrater reliability estimates were slightly higher than the intra-rater reliability, which indicates rater-dependent deviations in the placement of landmarks despite a standardized workflow.

In the literature, deviations were reported to be mostly caused by rater errors during the placement of anthropometric landmarks[74]. In our study sample, the greatest MAD were 2.013 mm in distance measurements, 1.471 degree in angular measurements, and 0.065 in ratio measurements for inter-rater agreement. However, their correspondent REM value were smaller than 3.9%. One conjecture regarding the large MAD values is the wide range from pairs of measurements with small and large values. The MAD of a large distance must always be related to its REM. The highest inter-rater agreement was in the TFCA measurement. Almost all agreements between measurements were above 0.75 based on ICC results. These findings were consistent with the intra-rater reliability. The ICC of most measurements for intra-method reliability was higher than 0.95 except for the NOAI with 0.948. The excellent results of the intra-method assessment demonstrated the high reliability of the 3D imaging system. Considering the intra- and

inter-rater reliability, the landmarks determination and placement protocol has been evaluated thoroughly and provides an effective reference for further comparative and clinical research.

Reliability is one of the most commonly used indicators to evaluate the errors generated in the validation of a novel measurement process. Reliability is the overall consistency of a measure. If it produces similar results under consistent conditions or the results are consistent from one testing occasion to another, this measure has higher reliability[72]. Determining both intra- and inter-rater reliability is important in evaluating the accuracy of measurement data. In this study, we used the five most commonly used estimates (MAD, REM, TEM, rTEM, ICC) based on former research to assess for avoiding the interference of terminology and make it easier for readers to understand[67,69, 75,76].

We also explored the reproducibility of these soft tissue landmarks on the 3D facial images in our two ethnic groups. The reproducibility of facial landmarks has been further validated in the three space planes. Our measurement results showed that the majority coordinates in x,y,z axes of the 46 landmarks could be reproducible to less than 1mm, which is clinically acceptable (87% intra-rater and 73.2% inter-rater). The reproducibility of the intra-rater evaluation was higher than the inter-rater. In ethnic subgroups, the measurement differences between intra-group and inter-group of landmarks in Asians were generally smaller than in Caucasians. The most reproducible and least reproducible landmarks among Asians were consistent with those among Caucasians. In the gender subgroup, landmarks focused on nose and mouth had higher reproducibility in males compared to females. While landmarks in the eye region had poorer reproducibility in males, bias between intra- and inter-rater in males were less than that in females. In both female and male groups, the Prn was the most reproducible landmark, while the landmark left Zy was the least reproducible.

5.3 Significance

5.3.1 Consistence

Our study found a good agreement between 3D-derived anthropometric measurements with the set landmark-based approach. The results demonstrated that most landmarks on 3D images obtained with the VECTRA XT stereophotogrammetry system, including the inter-landmarks distance and angles, were highly reliable. We found that the intra-method measurements had the highest reliability, followed by the intra-rater and inter-rater ones. The greatest deviations mainly concentrated on the nasal tip and around the nostrils. The reason might be that there was no consensual definition of tip border and the shortest distance perpendicular to the nostril long axis in a 3D image. These led to various identification of TDP and nostril short axis by different raters. Besides, variables with smaller measurement sizes tended to produce higher REM and ICC values in intra- and inter-rater reliability. Nevertheless, most of their intra- and inter-rater reliability showed good agreement within the ICC limits.

In a similarly designed study, Weinberg *et al.*[77] compared 3D anthropometric measurements on mannequin heads, but without test subjects. They discovered that the differences in the linear distances consistently stayed below 1mm. Our study showed deviations above 1 mm for selected measurements such as facial width and nasal length. However, these were concentrated at distances with a large amplitude, resulting in a MAD above 1mm, although the REM remained small and should not be clinically relevant. Besides, the examination of test subjects, in comparison to mannequin heads, could increase the variability and error due to subtle changes in facial expression and more complex surface properties. Menezes *et al.*[78] found that the results from the stationary Vectra system ranged from 0.13 to 1.19mm among repeated measurements

of the facial area. Based on previous studies, an error less than 2mm was generally considered accurate and precise enough for the validation of 3D photogrammetry. Whereas a deviation of 1 to 2mm may became relevant, for example, when high-precision measurements were required. For a more precise differentiation, we have used various previous studies to determine the focus of the eyes, facial proportions, nose, lips, and general facial measurements[79-83].

5.3.2 Influencing Factors

Based on our measurements in different sessions of intra-rater and inter-rater, we inferred the following criteria involved in the reliability and reproducibility of facial landmarks. First, the clear description and definition of landmarks. Second, the morphology and contour of the facial area where the landmark is located. Landmarks located in more convex or well-defined areas have higher reproducibility. For instance, Prn and TDP are more reproducible than Zy, which is located on a flatter site. Third, the feature and character of the landmark. The landmarks with distinct feature usually have higher reproducibility. Four, the ethnicity and gender with different characteristics of the facial surface. Five, rater dependency. For example, the degree of attention, discipline and consistency, 3D imaging software proficiency, and the knowledge of facial anatomy. Six, the quality of 3D imaging. The landmarks on the areas free of artifacts and defects are more reproducible.

5.3.3 Difference and Diversity

In addition, the reproducibility of our landmarks differed in three planes. That is to say, certain landmarks were harder to locate accurately in one axis than the other two.

Similar results were reported in former research[82-83]. Medelnik et al. attributed this bias to the position of landmarks relative to the individual's facial morphology[84]. The landmarks with poor reproducibility were concentrated on nose Al, chin, Tri, and Zy mostly. Raters may not find a suitable reference point in less clearly demarcated areas. Hair-bearing skin areas, such as the hairline, usually had lower reproducibility[85]. Moreover, it has been reported that the patient's head occasionally needed to be tilted back slightly to ensure data quality in nose and chin area, which made it complicated to ensure a consistent recording position[86]. Therefore, precautions should be taken in preparation for 3DSI to minimize the errors caused by hair and sitting positions, making the identification of landmarks more precise.

Some landmarks and coordinates varied by ethnicity. Landmarks distributed at the nasal tip and nostrils, such as Nl, Nb, Nt, Nm, TDP, Stb, and Prn were more reproducible in Caucasian species. Nasal anatomical features of Caucasians differ from those of Asians. A former study has found that the Caucasian descent typically had relatively thick nasal skin, straighter dorsum, more pronounced nasal tip, and teardrop shape nostrils. Correspondingly, the bony vault in Asians was usually wide and short. The dorsal aesthetic lines were not clearly defined, resulting in a less well-defined TDP. The nasal tip was widened with wide alar bases. The nasal length was shortened, with diminished tip projection and horizontally oriented nostrils[87]. These factors could impact the raters to identify the nasal tip and the axis of nostril and to locate the landmarks associated with these regions in Caucasians. Thus, before clinical use of a 3D landmark-based study, the reliability of the measurements for different ethnicities would need to be investigated separately.

We also observed few gender-dependent differences in landmark placement accuracy. In the intra-and inter-rater reproducibility assessment, the landmark Zy on both sides of the x-axis produced fewer errors in males. According to our observations, the zygomatic bone of male was larger and protruding than that of female, which facilitated the rater's positioning of Zy on the x-axis. Previous anthropometric studies showed that the chin and jawbones of male are more angular than that of female with the male's jaws are on average 17% higher vertically and have a more lateral fullness which may impact the 3D placement of landmarks in these areas[88]. These features may made it easier to locate the landmarks Ls, Li, Me, and C.

5.4 Limitations

The main limitation of our study is a small and diverse group with overall young patients which did not allow a refined investigation in different age groups.

Although distances and angles of inter-landmark measurements were calculated via the Canfield software, small artifacts in the endocanthion, forehead, and nostril region generated by the eyelash, hair, and vibrissae of volunteers, may cause deviation in measurement. This is a known limitation for almost all 3D surface scanners.
Furthermore, despite manual soft-tissue landmark placement in addition to automated landmark placement with the Vectra software, examiner-dependent errors cannot be completely excluded. Through a standardized procedure and training, the error was tried to be kept as minor as possible.

In addition, the Vectra XT system used in this study costs about 37.000 Euros which limits its wide application in normal clinical practice.

Nevertheless, despite its limitations, 3D photogrammetry still has a high potential for broad application in predicting soft tissue contours and monitoring treatment progress, especially for complex rhinoplasty and maxillofacial plastic surgery patients, and for the consultation of orthodontic treatment or orthognathic surger[89-93].

Future research should recruit more diversified participants to evaluate the reliability of 3D digital stereophotogrammetry in subjects in a wider age range or in more different races.

6 Summary

Before being widely used in clinics, the reliability of measurements based on facial landmarks should be inspected. This research introduces a detailed 3D digital nasal and perinasal anthropometry technology and proves its high reliability for analysis of nasal morphological features. It offers essential evidence and initial reference for the application of 3D nasal anthropometry in clinical practice. Compared to previous studies in oral and maxillofacial area on mannequins or the comparison of different 3D stereo imaging system on individuals, our study is closer to the clinical practice[11,37]. Moreover, we verified the reproducibility of each facial landmark should be on the x, y, and z three planes. In order to obtain good reproducibility, raters who place landmarks must clearly define and thoroughly understand their definitions. Landmarks located at different positions on the face have broad variation in reproducible levels. The landmarks placed on clear features and boundaries area have higher reproducibility than those placed on flat or a gently curved plane. This may be related to gender and ethnic differences in

facial morphology, leading to variations in the reproducibility of certain landmarks. Furthermore, it is also essential for raters to have sufficient knowledge of facial anatomy and proficiency in 3D images to improve the reproducibility of landmarks. In this study, the majority of the 138 coordinates from 46 facial landmarks had a reproducibility of less than 1mm, which is clinically acceptable (87% intra-rater and 73.2% inter-rater). The above results show that the cephalometry based on facial soft tissue landmarks can be used for surgical planning and evaluation of postoperative effects in the field of otolaryngology, plastic and cosmetic surgery, and maxillofacial surgery that need to change nasal morphology.

7 References

1. Sassouni, V. A roentgenographic cephalometric analysis of cephalo-faciodental relationships. Angle Orthod. 1955; 16: 735-765
2. Cobb, J. A projected grid method for recording the shape of the human face. Royal Aircraft Establishment, Techn. Rep. 71184, Farnborough (1971).
3. Robertson, N. Contour photography. Brit J Orthodont 1976; 3: 105-109
4. Leivesley, W. The reliability of contour photography for facial measurements. Brit J Orthodont. 1983; 10: 34-37
5. Burke PH, Beard LFH. Stereophotogrammetry of the face. Am J Orthodont.1971; 53: 769-782
6. Beckmann-van der Ven G, Segner D, Hasund A. Representation of the facial soft tissue surface in 3 dimensions with special reference to the mandible. Fortschr Kieferorthop. 1985 Aug;46(4):279-87.
7. Tzou CHJ , Artner NM , Pona I , et al. Comparison of three-dimensional surface-imaging systems. J Plast Reconstr Aesthetic Surg. 2014; 67(4):489-97 .

8. Seminati E, Talamas DC, Young M, et al. Validity and reliability of a novel 3D scanner for assessment of the shape and volume of amputees' residual limb models. PLoS One. 2017 Sep 8;12(9):e0184498.
9. Verhulst A, Hol M, Vreeken R, et al. Three-Dimensional Imaging of the Face: A Comparison Between Three Different Imaging Modalities. Aesthet Surg J. 2018 May 15;38(6):579-585.
10. Yongwei G, Xiaoyi H, Rokohl AC, et al. Reliability of Periocular Anthropometry: A Comparison of Direct, 2-Dimensional, and 3-Dimensional Techniques. Dermatol Surg. 2020 Sep;46(9): e23-e31.
11. Fourie Z , Damstra J , Gerrits PO , et al. Evaluation of anthropometric accuracy and reliability using different three-dimensional scanning systems. Forensic Sci Int. 2011 Apr 15;207(1-3):127-34
12. Khambay B , Nairn N , Bell A , et al. Validation and reproducibility of a high-resolution three-dimensional facial imaging system. British Journal of Oral & Maxillofacial Surgery, 2008, 46(1):1-32.
13. Weinberg SM , Naidoo S , Govier DP , et al. Anthropometric Precision and Accuracy of Digital Three-Dimensional Photogrammetry. Journal of Craniofacial Surgery, 2006, 17(3):477-483.
14. Koban KC, Härtnagl F, Titze V, et al. Chances and limitations of a low-cost mobile 3D scanner for breast imaging in comparison to an established 3D photogrammetric system. J Plast Reconstr Aesthet Surg. 2018 Oct;71(10):1417-1423.
15. Etzel L, Koban KC, Li Z, et al. Whole-body surface assessment - implementation and experiences with 360° 3D whole-body scans: opportunities to objectively monitor the extremities and the body trunk. Handchir Mikrochir Plast Chir. 2019 Aug;51(4):240-248.
16. Koban KC, Titze V, Etzel L, et al. Quantitative volumetric analysis of the lower extremity: validation against established tape measurement and water displacement. Handchir Mikrochir Plast Chir. 2018 Dec;50(6):393-399.

17. Koban KC, Frank K, Etzel L, et al. 3D Mammometric Changes in the Treatment of Idiopathic Gynecomastia. Aesthetic Plast Surg. 2019 Jun;43(3):616-624.
18. Koban KC, Etzel L, Li Z, et al. Three-dimensional surface imaging in breast cancer: a new tool for clinical studies? Radiat Oncol. 2020 Feb 28;15(1):52.
19. Garyfalia L, Peter C, Grant SH, et al. Evolution of Preoperative Rhinoplasty Consult by Computer Imaging. Facial Plast Surg. 2016 Feb;32(1):80-7
20. Villanueva NL, Afrooz PN, Carboy JA, Rohrich RJ. Nasal Analysis: Considerations for Ethnic Variation. 2019 Jun;143(6)
21. H Ghoddousi, R Edler, P Haers, D Wertheim, D Greenhill. Comparison of three methods of facial measurement. Int J Oral Maxillofac Surg. 2007 Mar;36(3):250-8.
22. Yongwei Guo, Xiaoyi Hou, Alexander C Rokohl, Renbing Jia, Ludwig M Heindl. Reliability of Periocular Anthropometry: A Comparison of Direct, 2-Dimensional, and 3-Dimensional Techniques. Dermatol Surg. 2020 Sep;46(9):e23-e31
23. Aung SC, Ngim RC, Lee ST. Evaluation of the laser scanner as a surface measuring tool and its accuracy compared with direct facial anthropometric measurements. Br J Plast Surg.1995;48:551–558.
24. Feng Z, Guiyang Z, Weijie F, et al. Application of 3D Printing Technology in RGPCL Simulation Fitting. Med Hypotheses. 2018;113 (1): 74-76.
25. Toriumi DM, Dixon TK. Assessment of rhinoplasty techniques by overlay of before-and-after 3D images. Facial Plast Surg Clin North Am. 2011 Nov;19(4):711-23 2016;32(1):80-7.
26. Farkas LG. Accuracy of anthropometric measurements: past, present, and future. Cleft Palate Craniofac J.1996;33:10-18
27. Möllhoff N, Koban KC, Engelhardt TO, et al. Case report of frontobasal reconstruction and volume augmentation using a free gracilis muscle flap and autologous fat grafting: utilising the free flap as a scaffold for fat transplantation. Handchir Mikrochir Plast Chir. 2020 Aug;52(4):330-334.

28. Savran A, Alyüz N, Dibeklioğlu H, et al. Bosphorus Database for 3D Face Analysis. Biometrics and Identity Management. Berlin, Germany: Springer, 2008:47-56
29. Xi Z, Dell AE, Liming C, et a. Accurate Landmarking of Three—dimensional Facial Data in the Presence of Facial Expressions and Occlusions using a Three-dimensional Statistical Facial Feature Model. IEEE Transactions on Systems, Man, and Cybernetics, Part B: Cybernetics, 2011; 41(5):1417-1428
30. Koban KC, Perko P, Etzel L, et al. Validation of two handheld devices against a non-portable three-dimensional surface scanner and assessment of potential use for intraoperative facial imaging. J Plast Reconstr Aesthet Surg. 2020 Jan;73(1):141-148.
31. Koban KC, Schenck T, Metz PM, Volkmer E, Haertnagl F, Titze V, Giunta RE. En Route for Objective Evaluation of Form, Volume, and Symmetry in Plastic Surgery using 3-D Intraoperative Scans. Handchir Mikrochir Plast Chir. 2016 Apr;48(2):78-84.
32. Guo HM, Wang KM, Ma JG. Application and prospect of 3D imaging and printing technology in rhinoplasty. Chin J Aesth Plast Surg, 2020 Sep; Vol. 31, No. 9
33. Prince JL and Links JM. Medical Imaging Signals and Systems. 2006, Pearson Prentice Hall
34. Yokozeki S. Moiré fringes. Optics and Lasers in Engineering. 1982, Vol 3, Issue 1:15-27
35. Lay YL, Yang HJ, Lin CS, et al. 3D Face Recognition by Shadow Moiré, Optics & Laser Technology.2012, Vol.44,No.1:148-152.
36. Franca JGDM, Gazziro MA, Ide NA, et al. A 3D scanning system based on laser triangulation and variable field of view. IEEE International Conference on Image Processing 2005. 2005, pp. I-425-428.
37. Zhang, S. High-speed 3D shape measurement with structured light methods: A review. Opt. Lasers Eng.2018, 106, 119–131.
38. Cotofana S, Koban KC, Konstantin F, et al. The Surface-Volume Coefficient of the Superficial and Deep Facial Fat Compartments: A Cadaveric Three-Dimensional Volumetric Analysis. Plast Reconstr Surg. 2019 Jun;143(6):1605-1613.

39. Koban KC, Cotofana S, Frank K, et al. Precision in 3-Dimensional Surface Imaging of the Face: A Handheld Scanner Comparison Performed in a Cadaveric Model. Aesthet Surg J. 2019 Mar 14;39(4): 36-44.
40. Heike, C. L, Upson, K, Stuhaug, E, et al. 3D digital stereophotogrammetry: a practical guide to facial image acquisition. Head Face Med. 2010,6,18.
41. Metzler P, Sun Y, Zemann W, et al. Validity of the 3D VECTRA photogrammetric surface imaging system for cranio-maxillofacial anthropometric measurements. Oral Maxillofac Surg. 2014,18:297-304
42. Lekakis G, Hens G, Clases P, et al. Three- dimensional morphing and its added value in the rhinoplasty consult. Plast Reconstr Surg Glob, 2019,7(l):e2063
43. Bechtold TE, Göz TG, Schaupp E, et al. Integration of a maxillary model into facial surface stereophotogrammetry. J Orofac Orthop.2012; 73:126–137
44. White JD, Castrillon AO, Virgo C, et al. Sources of variation in the 3dMDface and Vectra H1 3D facial imaging systems. Sci Rep. 2020 Mar 10;10(1):4443.
45. Daniele G, Valentina P, Annalisa C, et al. Are Portable Stereophotogrammetric Devices Reliable in Facial Imaging? A Validation Study of VECTRA H1 Device? J Oral Maxillofac Surg. 2018; 76(8):1772-1784.
46. Proffit WR, White RP, Sarver DM. Contemporary Treatment of Dentofacial Deformity. St. Louis: CV Mosby Co; 2003.
47. Koudelovea J, Bruzek J, Caganova V, et al: Development of facial sexual dimorphism in children aged between 12 and 15 years: A three-dimensional longitudinal study. Orthod Craniofac Res. 2015; 18:175
48. Pucciarelli V, Bertoli S, Codari M, et al: The face of Glut1-DS patients: A 3D craniofacial morphometric analysis. Clin Anat. 2017;30:644
49. Persing S, Timberlake A, Madari S, et al. Three-Dimensional Imaging in Rhinoplasty: A Comparison of the Simulated versus Actual Result. Aesthetic Plast Surg, 2018,42 (5): 133 1- 1335.

50. Khan G, Choi YS, Park ES, et al. The application of three- dimensional simulation program and three- dimensional printing in secondary rhinoplasty[J]. J Craniofac Surg, 2018,29(8) e774-e777.
51. Jung JW, Ha DH, Kim BY, et al. Nasal Reconstruction Using a Customized Three-Dimensional-Printed Stent for Congenital Arhinia: Three-Year Follow-up. Laryngoscope. 2019 Mar, 129(3):582-585.
52. López Gualdrón CI, Bravo Ibarra ER, Bohórquez Murillo AP, et al. Present and future for technologies to develop patient- specific medical devices: a systematic review approach. Med Devices (Auck I), 2019, 12:253-273
53. Koban KC, Leitsch S, Holzbach T, et al.3D-imaging and analysis for plastic surgery by smartphone and tablet: an alternative to professional systems? Handchir Mikrochir Plast Chir. 2014 Apr;46(2):97-104.
54. Kayastha D, Vakharia KT. The evolving roles of computer-based technology and smartphone applications in facial plastic surgery. Curr Opin Otolaryngol Head Neck Surg. 2019, 08;27(4):267-273.
55. Codazzi D, Bruschi S, Mazzola RF, et al. Bergamo 3D Rhinoplasty Software: Select, Store, and Share Surgical Maneuvers in a Three-Dimensional Nasal Model. Plast Reconstr Surg. 2016 Feb;137(2):313e-317e.
56. Guo, Y. et al. Reliability of periocular anthropometry using three-dimensional digital stereophotogrammetry. Graefe's Arch. Clin. Exp. Ophthalmol. 2019. 257, 2517–2531
57. Baik HS, Jeon JM, Lee HJ. Facial soft-tissue analysis of Korean adults with normal occlusion using a 3-dimensional laser scanner. Am J Orthod Dentofacial Orthop. 2007; 131:759–766
58. Bechtold TE, Göz TG, Schaupp E et al. Integration of a maxillary model into facial surface stereophotogrammetry. J Orofac Orthop. 2012; 73:126–137
59. Dindaroğlu F, Kutlu P, Duran GS, et al. Accuracy and reliability of 3D stereophotogrammetry: A comparison to direct anthropometry and 2D photogrammetry.

Angle Orthod. 2016; 86(3):487-94.

60. Khambay B, Nairn N, Bell A, et al. Validation and reproducibility of a high-resolution three-dimensional facial imaging system. Br J Oral Maxillofac Surg. 2008; 46(1):27-32.
61. Toma AM, Zhurov A, Playle R, et al. Reproducibility of facial soft tissue landmarks on 3D laser-scanned facial image. Orthod Craniofac Res. 2009;12(1):33-42.
62. Farkas LG. Examination. In: Farkas LG, ed. Anthropometry of the Head and Face, 2nd ed. New York: Raven Press, 1994:3–56
63. Swennen GR et al. Three-Dimensional Cephalometry: A color Altas and Manual. Springer Press,2006
64. Jamilian A, Darnahal A, Hamedi R et al. Photogrammetric analysis of facial profile in Persian adults. Gen Dent.2016;64(2):52-5.
65. Julian B Woelfel, Takayoshi Igarashi, Jin-Keun Dong. Faculty-supervised measurements of the face and of mandibular movements on young adults. J Adv Prosthodont. 2014;6(6):483-90.
66. Koepsell T, Weiss N. Epidemiologic Methods: Studying the Occurrence of Illness. Oxford: Oxford University Press; 2003.
67. Ulijaszek S, Kerr D. Intra- and inter-observer error in anthropometric measurement. In: Ulijaszek S, Mascie-Taylor C, eds. Anthropometry: The Individual and the Population. Cambridge, United Kingdom: Cambridge University Press; 1994:30–55.
68. Weinberg SM, Scott NM, Neiswanger K, Brandon CA, Marazita ML. Digital three-dimensional photogrammetry: Evaluation of anthropometric precision and accuracy using a Genex 3D camera system. Cleft Palate Craniofac J. 2004; 41:507 518
69. Andrade LM, Rodrigues da Silva AMB, Magri LV, et al. Repeatability study of angular and linear measurements on facial morphology analysis by means of stereophotogrammetry. J Craniofac Surg. 2017,28:1107–1111.
70. Camison L, Bykowski M, Lee WW, et al. Validation of the Vectra H1 portable three-dimensional photogrammetry system for facial imaging. Int J Oral Maxillofac Surg 2018,

47:403–410.

71. Perini TA, de Oliveira GL, Ornellas JS, de Oliveira FP. Technical error of measurement in anthropometry. Rev Bras Med Esporte 2005; 11: 86-90.
72. Toma AM, Zhurov A, Playle R, et al. Reproducibility of facial soft tissue landmarks on 3D laser-scanned facial image. Orthod Craniofac Res. 2009;12(1):33-42.
73. Fink M, Medelnik J, Strobel K. Metric precision via soft-tissue landmarks in three-dimensional structured-light scans of human faces. J Orofac Orthop. 2014 ;75(2):133-43.
74. Han L, Ping Z, Yi L, Yuxi Z, Yue X. Reliability and reproducibility of landmarks on three-dimensional soft-tissue cephalometric using different placement methods. Plast Reconstr Surg. 2014;134(1):102-110.
75. William M.K. Trochim. The Research Methods Knowledge Base.2007
76. Heike CL, Cunningham ML, Hing AV, Stuhaug E, Starr JR Picture perfect? Reliability of craniofacial anthropometry using three-dimensional digital stereophotogrammetry. Plast Reconstr Surg. 2009; 124:1261–1272.
77. Weinberg SM, Naidoo S, Daniel P et al. Govier Anthropometric precision and accuracy of digital three-dimensional photogrammetry: comparing the Genex and 3dMD imaging systems with one another and with direct anthropometry. J Craniofac Surg. 2006;17(3):477-83.
78. MD Menezes, R Rosati, VF Ferrario et al. Accuracy and reproducibility of a 3-dimensional stereophotogrammetric imaging system. J Oral Maxillofac Surg. 2010;68(9):2129-35.
79. Jinhua L, Alexander CR, Yongwei G et al. Reliability of Stereophotogrammetry for Area Measurement in the Periocular Region. Aesthetic Plast Surg. 2021 Jan 15
80. JB Woelfel, T Igarash, JK Dong. Faculty-supervised measurements of the face and of mandibular movements on young adults. J Adv Prosthodont. 2014 12;6(6):483-90.
81. AS Ketcham, Eric J Dobratz. Normal and variant anatomy of the nasal tip. Facial Plast Surg. 2012;28(2):137-44.

82. De Oliveira AE, Cevidanes LH, Phillips C et al. Observer reliability of three-dimensional cephalometric landmark identification on cone-beam computerized tomography. Oral Surg Oral Med Oral Pathol Oral Radiol Endod. 2009;107:256–265
83. Park SH, Yu HS, Kim KD et al. A proposal for a new analysis of craniofacial morphology by 3-dimensional computed tomography. Am J Orthod Dentofacial Orthop. 2006; 129:600. e23–600.e34
84. Medelnik J, Hertrich K, Steinhäuser-Andresen S et al. Accuracy of anatomical landmark identification using different CBCT- and MSCT-based 3D images. An in vitro study. J Orofac Orthop. 2011; 72:261–278
85. Berneburg M, Schubert C, Einem C, et alThe reproducibility of landmarks on three-dimensional images of 4- to 6-year-old children. J Orofac Orthop. 2010; 71:256–264
86. Heike CL, Upson K, Stuhaug E, Weinberg SM. 3D digital stereophotogrammetry: a practical guide to facial image acquisition. Head Face Med 2010; 6:18
87. Villanueva NL, Afrooz PN, Carboy JA, Rod J Rohrich et al. Nasal Analysis: Considerations for Ethnic Variation. Plast Reconstr Surg. 2019;143(6):1179e-1188e.
88. Ousterhout DK. Dr. Paul Tessier and facial skeletal masculinization. Ann Plast Surg. 2011 12;67(6):S10-5.
89. Singh P, Pearlman S. Use of Computer Imaging in Rhinoplasty: A Survey of the Practices of Facial Plastic Surgeons. Aesthetic Plast Surg. 2017 Aug;41(4):898-904.
90. Rho Nk, Park JY, Youn CS et,al. Early Changes in Facial Profile Following Structured Filler Rhinoplasty: An Anthropometric Analysis Using a 3-Dimensional Imaging System. Dermatol Surg. 2017 Feb;43(2):255-263.
91. Li WB, Liang Y, Sun Y, et al. Application of Three-Dimensional Imaging in Asian Rhinoplasty with Costal Cartilage. Aesthetic Plast Surg. 2021 Jan 11.
92. Othman SA, Saffai L, Hassan WNW. Validity and reproducibility of the 3D VECTRA photogrammetric surface imaging system for the maxillofacial anthropometric measurement on cleft patients. Clin Oral Investig. 2020 Aug;24(8):2853-2866.

93. Elnagar MH, Aronovich S, Kusnoto B. Digital Workflow for Combined Orthodontics and Orthognathic Surgery.Oral Maxillofac Surg Clin North Am. 2020 Feb;32(1):1-14.

8 Appendix

8.1 List of Figures

Figure 1. Vectra XT 3D Surface Imaging System 19

Figure 2. The standard position for an image capture with the Vectra XT 3D 20

Figure 3. The standard position for an image capture with the Vectra XT 3D.....22

Figure 4. Illustration of the landmarks used in this study (front view).....24

Figure 5. Illustration of the landmarks used in this study (isometric view) 25

Figure 6. Illustration of the landmarks used in this study (left and right side view) 25

Figure 7. Illustration of the landmarks used in this study (local perspective).....26

Figure 8. The measurements of projective linear distances 32

Figure 9. The measurements of surface linear distances 32

Figure 10. The measurements of Angles.....33

Figure 11. Intra-rater REM and rTEM across all nasal measurements on 3D images. (0.001% as one unit).....40

Figure 12. Inter-rater REM and rTEM across all nasal measurements on 3D images.....42

Figure 13. Inter-method REM and rTEM across all nasal measurements on 3D images.....44

Figure 14. Reproducibility of representative landmarks identification between Caucasian and Asian (intra-rater). 53

Figure 15. Reproducibility of representative landmarks identification between Female and Male (inter-rater).....54

8.2 List of Tables

Table 1. Demographic characteristics of study participants.....18

Table 2. The name and definition of facial landmarks used in this study 27

Table 3. List of 57 Nasal Measurements 29

Table 4. Summary of reliability estimates evaluated 35

Table 5. Overview of the reliability results of two raters 37

Table 6. Overall Reproducibility of identified landmarks.....46

Table 7. Rankings of facial soft tissue landmarks in Caucasian and Asian in respect to their reproducibility in the three spatial planes.....47

Table 8. Ranking of facial soft tissue landmarks in females and males in respect to their reproducibility in the three spatial planes.....50

9 Attachment

9.1 Tables

Table 1. The intra-rater reliability results

Variable	MAD	REM (%)	TEM	rTEM(%)	ICC (CI 95%)
NFRA	0.044	0.030	0.003	0.002	0.990 (0.985-0.994)
NLA	0.290	0.239	0.023	0.019	0.984 (0.975-0.990)
NDA	0.182	0.104	0.014	0.008	0.863 (0.786-0.912)
VNAr	0.124	0.281	0.010	0.022	0.937 (0.902-0.960)
VNAl	0.092	0.213	0.007	0.017	0.911 (0.861-0.943)
NA	0.053	0.055	0.004	0.004	0.960 (0.938-0.975)
SFAr	0.014	0.045	0.001	0.004	0.980 (0.969-0.987)
SFAl	0.169	0.565	0.013	0.045	0.983 (0.973-0.989)
MFAr	0.125	0.527	0.010	0.042	0.861 (0.784-0.911)
MFAl	0.051	0.212	0.004	0.017	0.931 (0.892-0.955)
IFAr	0.100	0.345	0.008	0.027	0.922 (0.878-0.950)
IFAl	0.052	0.178	0.004	0.014	0.937 (0.901-0.959)
TFCA	0.034	0.025	0.003	0.002	0.995 (0.992-0.997)
FCA	0.012	0.008	0.001	0.001	0.978 (0.966-0.986)
TRA	0.136	0.368	0.011	0.029	0.867 (0.793-0.915)
NOAr	0.121	0.243	0.010	0.019	0.812 (0.707-0.879)
NOAl	0.206	0.435	0.016	0.034	0.770 (0.645-0.854)
NTA	0.258	0.325	0.020	0.026	0.927 (0.886-0.953)
FW	0.758	0.641	0.060	0.051	0.956 (0.931-0.972)
FW2	0.124	0.072	0.010	0.006	0.993 (0.990-0.996)
FL	0.019	0.010	0.001	0.001	0.991 (0.985-0.994)
NRW	0.013	0.051	0.001	0.004	0.970 (0.953-0.981)
EnD	0.101	0.344	0.008	0.027	0.917 (0.871-0.947)
SSn	0.156	0.301	0.012	0.024	0.964 (0.945-0.977)
DBW	0.286	1.958	0.023	0.155	0.910 (0.860-0.942)
NL	0.035	0.053	0.003	0.004	0.959 (0.936-0.974)
NAAr	0.058	0.111	0.005	0.009	0.967 (0.948-0.979)
NAAl	0.173	0.330	0.014	0.026	0.957 (0.933-0.973)
DL	0.228	0.452	0.016	0.036	0.975 (0.961-0.984)
ABW	0.014	0.047	0.001	0.004	0.974 (0.960-0.984)
NBW	0.155	0.506	0.012	0.040	0.959 (0.936-0.974)

ALLr	0.193	0.609	0.015	0.048	0.940 (0.906-0.961)
ALLl	0.335	1.045	0.026	0.083	0.931 (0.892-0.956)
TW	0.188	1.881	0.015	0.149	0.874 (0.804-0.919)
TL	0.139	1.286	0.011	0.102	0.901 (0.845-0.936)
NSL	0.065	0.429	0.005	0.034	0.880 (0.813-0.923)
PRC	0.091	1.452	0.007	0.115	0.818 (0.716-0.883)
NLAr	0.008	0.055	0.001	0.004	0.974 (0.959-0.983)
NLAl	0.078	0.520	0.006	0.041	0.964 (0.944-0.977)
NSAr	0.077	1.152	0.006	0.091	0.975 (0.960-0.984)
NSAl	0.003	0.051	0.000	0.004	0.957 (0.933-0.973)
SSt	0.072	0.331	0.006	0.026	0.890 (0.828-0.929)
SMe	0.072	0.105	0.006	0.008	0.955 (0.929-0.971)
StM	0.006	0.012	0.000	0.001	0.952 (0.925-0.969)
CSn	0.065	0.429	0.005	0.034	0.880 (0.813-0.923)
GNS	0.100	0.647	0.008	0.051	0.863 (0.787-0.912)
DSL	0.216	0.473	0.017	0.037	0.975 (0.961-0.984)
NWI	0.001	0.556	0.000	0.111	0.964 (0.944-0.977)
NLI	0.000	0.047	0.000	0.004	0.945 (0.914-0.965)
DI1	0.002	0.243	0.000	0.019	0.855 (0.774-0.907)
DI2	0.004	0.352	0.000	0.028	0.945 (0.914-0.965)
NOI	0.001	0.242	0.000	0.019	0.869 (0.795-0.916)
DBI	0.008	1.627	0.001	0.129	0.854 (0.772-0.906)
TAR	0.008	0.803	0.001	0.064	0.811 (0.705-0.879)
NARr	0.006	0.284	0.001	0.022	0.976 (0.963-0.985)
NARl	0.013	0.516	0.001	0.04	0.977 (0.963-0.985)
NSI	0.004	0.526	0.000	0.04	0.832 (0.738-0.892)

Table 2. The inter-rater reliability results

Variable	MAD	REM (%)	TEM	rTEM (%)	ICC (CI 95%)
NFRA	0.397	0.275	0.031	0.022	0.973 (0.958-0.983)
NLA	0.993	0.820	0.065	0.054	0.946 (0.915-0.965)
NDA	0.669	0.384	0.053	0.030	0.774 (0.648-0.855)
VNAr	1.009	2.316	0.080	0.183	0.811 (0.706-0.879)
VNAl	1.400	3.293	0.111	0.260	0.829 (0.734-0.890)
NA	0.828	0.846	0.065	0.067	0.951 (0.924-0.969)
SFAr	0.362	1.224	0.029	0.097	0.929 (0.889-0.954)
SFAl	0.234	0.785	0.019	0.062	0.920 (0.875-0.948)
MFAr	0.366	1.524	0.029	0.120	0.899 (0.843-0.935)
MFAl	0.534	2.186	0.042	0.173	0.860 (0.782-0.910)
IFAr	0.346	1.206	0.027	0.095	0.801 (0.690-0.872)
IFAl	0.359	1.240	0.028	0.098	0.763 (0.631-0.848)

TFCA	0.789	0.574	0.062	0.045	0.985 (0.977-0.991)
FCA	1.471	0.895	0.116	0.071	0.959 (0.935-0.973)
TRA	0.479	1.308	0.038	0.103	0.843 (0.756-0.900)
NOAr	0.595	1.187	0.047	0.094	0.909 (0.859-0.942)
NOAl	0.546	1.148	0.043	0.091	0.937 (0.901-0.959)
NTA	0.216	0.272	0.017	0.021	0.933 (0.895-0.957)
FW	1.791	1.502	0.142	0.119	0.895 (0.836-0.932)
FW2	0.087	0.051	0.007	0.004	0.831 (0.736-0.891)
FL	0.364	0.195	0.029	0.015	0.976 (0.962-0.984)
NRW	0.694	2.690	0.055	0.213	0.942 (0.909-0.963)
EnD	0.003	0.010	0.000	0.001	0.808 (0.701-0.877)
SSn	1.158	2.213	0.092	0.175	0.878 (0.810-0.922)
DBW	0.906	6.395	0.072	0.506	0.893 (0.833-0.931)
NL	2.013	2.975	0.159	0.235	0.812 (0.707-0.880)
NAAr	0.878	1.661	0.069	0.131	0.878 (0.809-0.922)
NAAl	0.885	1.677	0.070	0.133	0.863 (0.786-0.912)
DL	1.063	2.296	0.084	0.182	0.880 (0.813-0.923)
ABW	0.610	1.986	0.048	0.157	0.970 (0.953-0.981)
NBW	0.150	0.490	0.012	0.039	0.849 (0.764-0.903)
ALLr	0.071	0.224	0.006	0.018	0.917 (0.871-0.947)
ALLl	0.147	0.461	0.012	0.036	0.914 (0.866-0.945)
TW	0.274	2.702	0.022	0.214	0.76 (0.626-0.846)
TL	0.139	2.041	0.161	1.481	0.732 (0.583-0.828)
NSL	0.662	4.292	0.052	0.339	0.915 (0.867-0.945)
PRC	0.067	1.069	0.005	0.085	0.864 (0.787-0.913)
NLAr	0.319	2.135	0.025	0.169	0.787 (0.669-0.864)
NLAl	0.205	1.358	0.016	0.107	0.972 (0.956-0.982)
NSAr	0.520	7.522	0.041	0.595	0.943 (0.912-0.964)
NSAl	0.317	4.933	0.025	0.390	0.855 (0.774-0.907)
SSt	0.979	4.620	0.077	0.365	0.808 (0.701-0.877)
SMe	1.373	2.004	0.109	0.158	0.847 (0.761-0.902)
StM	0.395	0.831	0.031	0.066	0.860 (0.782-0.910)
CSn	0.849	5.474	0.067	0.433	0.788 (0.670-0.864)
GNS	0.808	5.155	0.064	0.408	0.883 (0.818-0.925)
DSL	0.513	1.115	0.041	0.088	0.886 (0.822-0.927)
NWI	0.002	1.197	0.000	0.095	0.862 (0.785-0.912)
NLI	0.009	2.464	0.001	0.195	0.811 (0.705-0.879)
DI1	0.004	0.516	0.000	0.058	0.862 (0.784-0.911)
DI2	0.018	1.596	0.001	0.126	0.936 (0.900-0.959)
NOI	0.003	0.962	0.001	0.194	0.843 (0.755-0.899)
DBI	0.007	1.391	0.001	0.110	0.913 (0.864-0.944)
TAR	0.008	0.870	0.001	0.069	0.969 (0.952-0.980)
NARr	0.065	2.939	0.005	0.232	0.920 (0.876-0.949)
NARl	0.053	2.187	0.004	0.173	0.976 (0.963-0.985)
NSI	0.014	1.966	0.001	0.155	0.818 (0.717-0.883)

Table 3. The intra-method reliability results

Variable	Capture 1	Capture 2	MAD	REM	TEM	rTEM(%)	ICC
NFRA	144.075	144.673	0.598	0.414	0.047	0.033	0.998 (0.996-0.998)
NLA	121.58	121.725	0.145	0.119	0.011	0.009	0.996 (0.994-0.997)
NDA	174.779	174.87	0.091	0.052	0.007	0.004	0.968 (0.950-0.979)
VNAr	44.084	44.022	0.062	0.141	0.005	0.011	0.984 (0.975-0.990)
VNAl	43.198	43.152	0.046	0.106	0.004	0.008	0.978 (0.965-0.986)
NA	97.398	97.371	0.027	0.027	0.002	0.002	0.990 (0.985-0.994)
SFAr	29.783	29.776	0.007	0.023	0.001	0.002	0.995 (0.992-0.997)
SFAl	29.961	29.877	0.085	0.283	0.007	0.022	0.996 (0.993-0.997)
MFAr	23.824	23.886	0.063	0.263	0.005	0.021	0.965 (0.945-0.977)
MFAl	24.137	24.162	0.026	0.106	0.002	0.008	0.983 (0.973-0.989)
IFAr	28.907	28.957	0.05	0.172	0.004	0.014	0.981 (0.970-0.988)
IFAl	29.113	29.139	0.026	0.089	0.002	0.007	0.985 (0.976-0.990)
TFCA	136.921	136.904	0.017	0.012	0.001	0.001	0.999 (0.998-0.999)
FCA	163.642	163.648	0.006	0.004	0	0	0.995 (0.992-0.997)
TRA	36.847	36.779	0.068	0.184	0.005	0.015	0.966 (0.947-0.978)
NOAr	49.797	49.736	0.06	0.121	0.005	0.01	0.951 (0.923-0.969)
NOAl	47.341	47.238	0.103	0.218	0.008	0.017	0.948 (0.919-0.967)
NTA	79.451	79.322	0.129	0.163	0.01	0.013	0.982 (0.972-0.988)
FW	118.333	118.712	0.379	0.32	0.03	0.025	0.989 (0.983-0.993)
FW2	171.426	171.364	0.062	0.036	0.005	0.003	0.998 (0.997-0.999)
FL	186.334	186.343	0.009	0.005	0.001	0	0.998 (0.996-0.999)
NRW	26.151	26.145	0.007	0.025	0.001	0.002	0.992 (0.988-0.995)
EnD	29.29	29.239	0.05	0.172	0.004	0.014	0.979 (0.967-0.987)
SSn	51.751	51.829	0.078	0.151	0.006	0.012	0.991 (0.986-0.994)
DBW	14.623	14.48	0.143	0.984	0.011	0.078	0.979 (0.967-0.987)
NL	66.67	66.687	0.018	0.026	0.001	0.002	0.990 (0.985-0.994)
NAAr	52.41	52.439	0.029	0.056	0.002	0.004	0.992 (0.987-0.995)
NAAl	52.334	52.334	0	0	0	0	0.989 (0.983-0.993)
DL	45.771	45.88	0.108	0.236	0.009	0.019	0.994 (0.990-0.996)
ABW	30.431	30.424	0.007	0.023	0.001	0.002	0.994 (0.990-0.996)
NBW	30.589	30.512	0.077	0.253	0.006	0.02	0.998 (0.996-0.999)
ALLr	31.72	31.623	0.097	0.305	0.008	0.024	0.986 (0.978-0.991)
ALLl	32.042	31.875	0.167	0.524	0.013	0.041	0.984 (0.975-0.990)
TW	10.014	9.919	0.094	0.945	0.007	0.075	0.969 (0.952-0.980)
TL	10.824	10.755	0.07	0.645	0.006	0.051	0.975 (0.961-0.984)
NSL	15.093	15.125	0.032	0.214	0.003	0.017	0.970 (0.954-0.981)
PRC	6.264	6.219	0.045	0.729	0.004	0.058	0.953 (0.927-0.970)
NLAr	14.802	14.798	0.004	0.028	0	0.002	0.994 (0.990-0.996)
NLAl	14.997	15.036	0.039	0.26	0.003	0.021	0.991 (0.986-0.994)

NSAr	6.655	6.693	0.038	0.575	0.003	0.045	0.994 (0.990-0.996)
NSAl	6.277	6.275	0.002	0.025	0	0.002	0.989 (0.983-0.993)
SSt	21.675	21.711	0.036	0.165	0.003	0.013	0.973 (0.958-0.983)
SMe	69.199	69.235	0.036	0.052	0.003	0.004	0.989 (0.982-0.993)
StM	47.765	47.762	0.003	0.006	0	0	0.988 (0.982-0.992)
CSn	15.093	15.125	0.032	0.214	0.003	0.017	0.970 (0.954-0.981)
GNS	15.455	15.405	0.05	0.323	0.004	0.026	0.965 (0.945-0.978)
DSL	46.584	46.963	0.379	0.809	0.03	0.064	0.994 (0.990-0.996)
NWl	0.179	0.179	0	0.105	0	0.008	0.981 (0.971-0.988)
NLl	0.358	0.358	0	0.025	0	0.002	0.983 (0.974-0.989)
Dl1	0.776	0.777	0.001	0.122	0	0.01	0.963 (0.943-0.976)
Dl2	1.091	1.092	0.002	0.176	0	0.014	0.987 (0.979-0.992)
NOl	0.313	0.314	0	0.121	0	0.01	0.960 (0.937-0.974)
DBl	0.5	0.496	0.004	0.817	0	0.065	0.966 (0.947-0.978)
TAR	0.935	0.931	0.004	0.403	0	0.032	0.951 (0.923-0.968)
NARr	2.261	2.258	0.003	0.142	0	0.011	0.994 (0.991-0.996)
NARl	2.43	2.437	0.006	0.258	0	0.02	0.994 (0.991-0.996)
NSl	0.706	0.708	0.002	0.263	0	0.021	0.957 (0.932-0.972)

Table 6. Overall evaluation of the reproducibility of Caucasian and Asian facial soft tissue landmarks on three spatial planes.

Race	Caucasian (n=80)						Asian (n=80)					
Area	Landmarks	Axis	Intra-rater		Inter-rater		Landmarks	Axis	Intra-rater		Inter-rater	
			Mean	SD	Mean	SD			Mean	SD	Mean	SD
Nose	Nl l	x	0.15	0.15	0.42	0.26	Nl l	x	0.30	0.21	0.30	0.25
		y	0.13	0.12	0.22	0.14		y	0.09	0.08	0.21	0.20
		z	0.22	0.15	0.35	0.28		z	0.16	0.12	0.22	0.21
	Nl r	x	0.19	0.13	0.32	0.58	Nl r	x	0.22	0.19	0.32	0.29
		y	0.16	0.10	0.43	0.36		y	0.28	0.24	0.31	0.31
		z	0.15	0.12	0.52	0.39		z	0.21	0.18	0.18	0.13
	Nb l	x	0.24	0.16	0.50	0.46	Nb r	x	0.28	0.17	0.31	0.30
		y	0.20	0.14	0.41	0.61		y	0.20	0.13	0.20	0.19
		z	0.13	0.10	0.53	0.39		z	0.25	0.21	0.37	0.19
	Nb r	x	0.19	0.16	0.55	0.15	Nb l	x	0.32	0.35	0.38	0.22
		y	0.26	0.26	0.45	0.17		y	0.24	0.32	0.30	0.25
		z	0.17	0.34	0.42	0.13		z	0.26	0.21	0.45	0.35
	Nt r	x	0.25	0.16	0.39	0.21	Nt r	x	0.37	0.37	0.26	0.18
		y	0.14	0.04	0.45	0.40		y	0.32	0.26	0.28	0.21
		z	0.25	0.21	0.64	0.67		z	0.19	0.13	0.56	0.55
	Nt l	x	0.26	0.14	0.51	0.18	Nt l	x	0.31	0.25	0.50	0.35
		y	0.23	0.14	0.40	0.26		y	0.28	0.21	0.68	0.47
		z	0.19	0.17	0.68	0.34		z	0.63	0.53	0.10	0.06
	Nm l	x	0.27	0.19	0.53	0.18	Cc	x	0.58	0.54	0.71	0.62
		y	0.17	0.14	0.37	0.18		y	0.43	0.33	0.55	0.34

		z	0.30	0.24	0.71	0.50		z	0.21	0.19	0.24	0.17
	Nm r	x	0.30	0.21	0.35	0.27	Cm	x	0.28	0.12	0.38	0.27
		y	0.07	0.07	0.49	0.38		y	0.43	0.19	0.74	0.60
		z	0.34	0.25	0.75	0.71		z	0.54	0.23	0.61	0.49
	G	x	0.27	0.18	0.56	0.42	G	x	0.43	0.27	0.91	0.68
		y	0.20	0.13	0.83	0.44		y	0.51	0.50	0.44	0.42
		z	0.42	0.28	0.34	0.26		z	0.36	0.33	0.42	0.25
	Prn	x	0.35	0.23	0.79	0.51	Prn	x	0.54	0.34	0.50	0.48
		y	0.27	0.12	0.88	0.77		y	0.47	0.37	0.20	0.21
		z	0.30	0.26	0.33	0.23		z	0.28	0.24	0.96	0.74
	Cm	x	0.30	0.27	0.68	0.58	Al l	x	0.47	0.27	0.89	0.75
		y	0.41	0.24	0.99	0.68		y	0.62	0.94	0.26	0.20
		z	0.34	0.22	0.32	0.23		z	0.09	0.07	0.64	0.49
	Stb	x	0.41	0.31	0.92	0.63	Al r	x	0.59	0.53	0.81	0.49
		y	0.52	0.39	0.81	0.66		y	0.59	0.39	0.67	0.46
		z	0.08	0.08	0.59	0.33		z	0.54	0.46	0.63	0.36
	TDP r	x	0.60	0.58	0.48	0.31	TDP r	x	0.50	0.44	0.61	0.38
		y	0.32	0.25	1.37	1.08		y	0.57	0.43	1.05	0.90
		z	0.33	0.29	0.09	0.07		z	0.69	0.63	0.20	0.17
Nose	TDP l	x	0.53	0.50	0.40	0.28	TDP l	x	0.66	0.51	0.75	0.72
		y	0.45	0.35	1.16	0.79		y	0.68	0.60	0.73	0.65
		z	0.31	0.29	0.81	0.66		z	0.60	0.55	0.74	0.71
	Se	x	0.42	0.33	1.23	1.13	Se	x	0.59	0.51	0.65	0.46
		y	0.70	0.58	0.41	0.34		y	0.73	0.57	0.78	0.60
		z	0.17	0.15	0.79	0.55		z	0.70	0.79	0.84	0.66
	Cc	x	0.63	0.41	1.08	0.64	Nm r	x	0.60	0.52	0.90	0.68
		y	0.67	0.53	1.06	0.61		y	0.96	0.64	0.81	0.75
		z	0.10	0.08	0.47	0.38		z	0.38	0.24	0.55	0.42
	Ac l	x	0.53	0.37	0.80	0.76	Nm l	x	0.55	0.42	0.66	0.57
		y	0.62	0.50	1.03	0.75		y	0.98	0.90	0.73	0.64
		z	0.76	0.53	0.93	0.65		z	0.50	0.30	0.92	0.49
	Holn	x	0.57	0.35	1.07	0.89	Holn	x	0.57	0.58	0.46	0.29
		y	0.85	0.66	0.82	0.58		y	1.02	0.92	1.45	1.06
		z	0.57	0.31	1.09	0.55		z	0.66	0.55	0.76	0.63
	Ac r	x	0.57	0.39	1.05	0.77	Ac r	x	0.65	0.39	0.82	0.69
		y	0.78	0.59	0.99	0.78		y	1.12	0.90	1.14	0.83
		z	0.68	0.48	0.98	0.71		z	0.74	0.62	0.97	0.59
	Se'r	x	0.60	0.53	0.97	0.74	Se'r	x	0.76	0.59	0.69	0.57
		y	0.73	0.55	0.99	0.79		y	1.39	0.64	1.58	1.29
		z	0.72	0.55	1.12	0.61		z	0.25	0.16	0.13	0.08
	Se'l	x	0.34	0.24	1.05	0.69	Se'l	x	0.69	0.47	1.16	1.12
		y	1.06	1.09	1.11	0.74		y	1.35	1.11	0.85	0.69
		z	0.58	0.40	1.03	0.78		z	0.60	0.49	1.15	0.95
	N	x	0.72	0.40	0.99	0.57	N	x	1.01	0.65	0.70	0.52

		y	1.03	0.66	1.36	0.53		y	1.05	0.62	1.46	0.99
		z	0.08	0.06	0.77	0.39		z	0.76	0.52	0.93	1.00
	Al l	x	0.60	0.60	1.14	0.72	Ac l	x	0.80	0.57	0.99	0.43
		y	0.29	0.24	0.56	0.34		y	1.34	0.42	1.44	0.76
		z	1.12	0.83	1.39	0.87		z	0.50	0.38	0.71	0.18
Nose	Al r	x	0.68	0.54	0.98	0.43	Stb	x	0.56	0.52	0.84	0.60
		y	0.76	0.51	1.15	0.64		y	1.67	0.86	1.29	0.84
		z	0.80	0.60	1.19	0.78		z	0.39	0.37	1.13	0.66
	Sn	x	0.53	0.31	0.86	0.38	Sn	x	1.03	0.66	0.63	0.47
		y	1.16	0.86	1.46	0.57		y	1.47	1.31	1.46	1.12
		z	0.67	0.37	1.04	0.74		z	0.19	0.28	1.09	0.77
	Ort l	x	0.71	0.65	0.84	0.58	Ort l	x	1.13	0.89	0.55	0.66
		y	1.22	0.65	1.65	0.93		y	1.25	1.37	1.71	0.99
		z	0.66	0.49	0.88	0.63		z	0.66	0.42	0.78	0.64
	Ort r	x	0.61	0.48	1.04	0.91	Ort r	x	0.76	0.59	1.27	0.69
		y	1.32	0.89	1.52	1.08		y	1.39	0.84	1.20	0.86
		z	0.72	0.53	0.97	0.52		z	1.08	0.61	0.88	0.65
Eye	En r	x	0.43	0.27	0.45	0.32	En r	x	0.36	0.25	0.51	0.48
		y	0.51	0.36	0.71	0.51		y	0.37	0.28	0.68	0.42
		z	0.38	0.28	0.09	0.05		z	0.12	0.11	0.37	0.30
	En l	x	0.61	0.47	0.65	0.34	En l	x	0.51	0.36	0.88	0.76
		y	0.47	0.31	0.77	0.73		y	0.41	0.35	0.59	0.41
		z	0.35	0.18	0.50	0.36		z	0.11	0.14	0.47	0.32
	Em r	x	0.52	0.43	0.90	0.39	Em r	x	0.65	0.25	0.76	0.36
		y	0.69	0.14	0.53	0.34		y	0.74	0.66	0.93	0.57
		z	0.35	0.25	0.45	0.10		z	0.40	0.36	0.59	0.44
	Em l	x	0.87	0.87	1.24	1.00	Em l	x	0.82	0.76	1.02	0.64
		y	0.44	0.32	0.98	0.63		y	0.60	0.55	0.84	0.53
		z	0.42	0.25	0.46	0.40		z	0.34	0.29	0.65	0.47
Mouth	Sto	x	0.59	0.33	0.59	0.56	Sto	x	0.44	0.30	0.62	0.52
		y	0.43	0.28	0.59	0.37		y	0.61	0.31	0.82	0.64
		z	0.18	0.16	0.33	0.32		z	0.32	0.20	0.42	0.55
	Li	x	0.59	0.50	0.67	0.37	Li	x	0.50	0.47	0.71	0.38
		y	0.45	0.38	0.65	0.29		y	0.64	0.68	0.88	0.59
		z	0.09	0.06	0.36	0.29		z	0.23	0.29	0.28	0.24
	Ls	x	0.53	0.36	0.61	0.45	Ls	x	0.62	0.44	0.62	0.50
		y	0.52	0.42	0.57	0.42		y	0.72	0.49	0.87	0.70
		z	0.15	0.15	0.60	0.10		z	0.48	0.49	0.50	0.23
	Sm	x	0.67	0.57	0.82	0.45	Sm	x	0.78	0.57	0.97	0.68
		y	0.79	0.52	0.71	0.89		y	0.79	0.57	1.00	0.57
		z	0.14	0.12	0.37	0.35		z	0.10	0.10	0.23	0.12
	Sl	x	0.91	0.21	1.02	0.32	Sl	x	0.91	0.60	0.97	0.61
		y	0.90	0.75	0.95	0.69		y	0.74	0.71	0.82	0.52
		z	0.18	0.18	0.48	0.41		z	0.91	0.60	1.05	0.23

	Pg	x	0.80	0.57	1.18	0.76	Pg	x	1.01	0.77	1.02	0.89
		y	1.27	0.97	2.00	0.53		y	1.31	1.02	1.65	0.54
		z	0.78	0.54	0.94	0.64		z	1.28	1.25	1.16	0.86
	Me	x	1.06	0.99	1.64	0.92	Me	x	2.06	1.56	2.11	1.34
		y	0.87	0.79	0.81	0.72		y	0.71	0.58	0.97	0.71
		z	1.34	0.94	1.95	1.81		z	1.41	1.04	1.61	0.95
	C	x	1.22	0.55	1.13	0.74	C	x	1.15	0.95	1.51	0.95
		y	1.05	0.63	1.81	1.06		y	1.06	0.77	1.69	0.54
		z	1.98	1.20	2.16	1.67		z	2.11	1.07	1.95	0.47
Ear	Trg l	x	0.36	0.35	0.91	0.75	Trg l	x	0.30	0.24	0.40	0.35
		y	0.79	0.60	1.34	1.55		y	1.08	0.87	0.97	0.73
		z	1.06	0.74	1.26	1.13		z	1.08	0.80	1.49	0.99
	Trg r	x	0.40	0.36	0.67	0.62	Trg r	x	0.27	0.54	0.64	0.52
		y	0.84	0.68	1.43	0.73		y	0.86	0.75	1.28	0.90
		z	1.19	0.88	1.58	1.50		z	1.24	0.92	1.55	1.12
	Pa l	x	0.65	0.62	1.41	0.44	Pa l	x	0.32	0.21	0.55	0.51
		y	1.26	0.77	1.85	0.83		y	1.22	0.69	1.80	1.21
		z	0.64	0.45	1.48	0.61		z	0.88	0.63	1.70	0.93
	Pa r	x	0.63	0.47	0.97	0.36	Pa r	x	0.27	0.28	0.62	0.49
		y	1.57	0.95	1.75	0.91		y	1.48	1.43	1.84	1.12
		z	0.76	0.57	1.99	0.66		z	0.76	0.50	1.44	0.97
Other	Tri	x	1.03	1.05	1.60	1.15	Tri	x	1.01	0.78	1.11	0.93
		y	1.99	1.13	2.13	1.10		y	1.43	1.32	1.86	1.15
		z	1.37	1.12	2.04	0.87		z	1.22	0.61	1.21	0.87
	Zy r	x	1.31	0.90	1.61	1.03	Zy r	x	2.02	0.61	1.63	0.99
		y	2.08	1.17	2.21	1.11		y	2.13	1.52	2.57	1.28
		z	0.98	0.61	2.11	1.03		z	1.86	0.89	2.05	1.56
	Zy l	x	1.32	1.07	3.09	1.46	Zy l	x	1.65	1.02	1.55	0.73
		y	1.98	1.40	2.14	0.95		y	2.47	1.58	2.83	1.16
		z	2.00	1.61	2.45	1.10		z	1.91	1.09	2.05	1.37

Table 5. Overall evaluation of the reproducibility of female and male facial soft tissue landmarks on three spatial planes

Area	landmarks	Axis	Intra-rater		Inter-rater		landmarks	Axis	Intra-rater		Inter-rater	
			Mean	SD	Mean	SD			Mean	SD	Mean	SD
Nose	Prn	x	0.22	0.19	0.35	0.28	Prn	x	0.23	0.19	0.30	0.23
		y	0.30	0.26	0.34	0.18		y	0.23	0.23	0.30	0.17
		z	0.20	0.22	0.27	0.13		z	0.16	0.13	0.33	0.16
	Cm	x	0.28	0.25	0.26	0.19	Cm	x	0.26	0.22	0.28	0.11
		y	0.23	0.21	0.28	0.24		y	0.24	0.19	0.30	0.13
		z	0.22	0.17	0.46	0.35		z	0.17	0.17	0.37	0.17
	Holn	x	0.29	0.16	0.44	0.30	Holn	x	0.24	0.16	0.25	0.08
		y	0.24	0.14	0.29	0.22		y	0.20	0.13	0.29	0.13

		z	0.21	0.18	0.32	0.27		z	0.24	0.21	0.43	0.18
	TDP r	x	0.35	0.21	0.32	0.28	TDP r	x	0.26	0.21	0.34	0.19
		y	0.10	0.10	0.24	0.21		y	0.29	0.09	0.39	0.23
		z	0.38	0.31	0.45	0.25		z	0.27	0.24	0.33	0.17
	TDP l	x	0.29	0.20	0.42	0.25	TDP l	x	0.32	0.39	0.31	0.31
		y	0.09	0.07	0.40	0.39		y	0.30	0.69	0.73	0.53
		z	0.51	1.56	0.77	0.70		z	0.27	0.44	0.42	0.41
	Se	x	0.39	0.32	0.47	0.31	Se	x	0.40	0.44	0.33	0.24
		y	0.44	0.43	0.91	0.07		y	0.14	0.13	0.67	0.46
		z	0.32	0.38	0.10	0.09		z	0.32	0.30	0.51	0.35
	G	x	0.48	0.30	0.78	0.63	G	x	0.33	0.33	0.50	0.35
		y	0.47	0.40	0.25	0.24		y	0.37	0.21	0.84	0.68
		z	0.09	0.13	0.90	0.68		z	0.25	0.13	0.09	0.06
	Ac l	x	0.22	0.22	0.92	0.74	Ac l	x	0.28	0.22	0.72	0.79
		y	0.15	0.09	0.27	0.18		y	0.19	0.66	0.65	0.38
		z	0.61	1.58	0.93	0.48		z	0.52	0.35	0.35	0.31
	Ac r	x	0.41	0.25	0.84	0.66	Ac r	x	0.40	0.27	0.75	0.70
		y	0.24	0.17	0.88	0.46		y	0.52	0.48	0.53	0.54
		z	0.56	0.26	0.55	0.42		z	0.07	0.06	0.85	0.63
	Nt l	x	0.31	0.21	0.46	0.29	Nt l	x	0.34	0.13	0.79	0.41
		y	0.28	0.17	0.92	0.64		y	0.40	0.19	0.87	0.67
		z	0.62	0.51	0.91	0.70		z	0.43	0.31	0.41	0.21
	Nt r	x	0.40	0.30	0.73	0.52	Nt r	x	0.37	0.22	1.06	0.68
		y	0.53	0.49	0.96	0.63		y	0.40	0.26	0.56	0.39
		z	0.43	0.38	0.79	0.50		z	0.43	0.20	0.50	0.27
	Nl l	x	0.35	0.31	0.92	0.65	Nl l	x	0.45	0.50	0.96	0.82
		y	0.47	0.40	0.56	0.39		y	0.55	0.55	0.61	0.38
		z	0.57	0.55	0.98	0.68		z	0.37	0.25	1.04	0.65
	Nl r	x	0.54	0.40	0.91	0.65	Nl r	x	0.59	0.49	0.76	0.60
		y	0.53	0.54	0.93	0.85		y	0.44	0.53	0.74	0.67
		z	0.54	0.45	0.95	0.72		z	0.44	0.56	1.25	1.14
	Ort l	x	0.53	0.54	1.42	0.92	Ort l	x	0.54	0.30	1.35	1.32
		y	0.56	0.40	0.62	0.43		y	0.48	0.35	0.77	0.56
		z	0.62	0.38	0.50	0.34		z	0.52	0.22	0.86	0.79
	Ort r	x	0.64	0.31	0.59	0.42	Ort r	x	0.53	0.42	0.82	0.59
		y	0.53	0.33	1.51	0.94		y	0.45	0.37	0.80	0.58
		z	0.59	0.26	0.27	0.23		z	0.60	0.27	1.39	0.97
Nose	Cc	x	0.47	0.27	0.88	0.72	Cc	x	0.63	0.56	1.01	0.89
		y	0.94	0.65	1.14	0.88		y	0.84	0.73	1.26	0.88
		z	0.42	0.14	0.78	0.64		z	0.20	0.19	1.07	1.27
	Sn	x	0.82	0.62	0.68	0.49	Sn	x	0.50	0.33	0.64	0.49
		y	0.75	0.67	0.87	0.63		y	0.91	0.87	1.17	0.40
		z	0.25	0.41	0.97	0.14		z	0.38	0.34	1.06	0.74

	Se'l	x	0.51	0.42	0.74	0.57	Se'l	x	0.43	0.42	0.49	0.28
		y	0.97	0.82	0.84	0.68		y	0.98	1.05	1.91	1.53
		z	0.30	0.24	1.42	0.67		z	0.35	0.19	0.38	0.26
	Se'r	x	0.56	0.37	0.59	0.37	Nb l	x	0.49	0.38	0.55	0.53
		y	0.69	0.22	1.75	1.02		y	0.64	0.45	1.98	0.61
		z	0.85	0.90	0.35	0.29		z	0.96	0.60	0.27	0.24
	Nb l	x	0.78	0.71	0.42	0.35	Nb r	x	0.59	0.50	0.69	0.53
		y	0.70	1.02	0.98	0.63		y	0.64	0.56	1.55	0.99
		z	0.71	0.61	1.64	0.81		z	0.91	0.75	1.36	0.98
	Nb r	x	0.53	0.38	0.84	0.96	Se'r	x	0.85	0.55	1.65	1.32
		y	0.70	0.51	1.19	0.83		y	0.96	0.62	1.03	0.77
		z	0.95	0.93	1.52	1.21		z	0.19	0.28	1.27	0.78
	Nm l	x	0.90	0.58	0.98	0.59	Nm l	x	0.57	0.41	1.00	0.81
		y	1.04	0.78	1.50	0.44		y	1.09	0.81	1.87	1.44
		z	0.10	0.10	1.38	0.38		z	0.61	0.39	0.96	0.53
	Nm r	x	0.72	0.50	1.00	0.64	Nm r	x	0.78	0.60	1.35	0.66
		y	0.94	0.73	1.81	1.07		y	0.81	0.83	1.83	0.87
		z	0.85	0.29	0.91	0.71		z	0.83	0.76	0.96	0.70
Nose	Al r	x	0.82	0.43	1.08	0.86	Al r	x	0.60	0.48	1.26	1.11
		y	0.96	0.67	2.29	1.41		y	1.01	0.77	2.00	1.42
		z	0.74	0.55	0.97	0.63		z	0.90	0.57	1.08	0.69
	Al l	x	0.76	0.52	0.96	0.73	Al l	x	0.80	0.68	1.63	1.14
		y	1.09	1.16	2.48	1.53		y	1.01	0.41	0.93	0.85
		z	0.67	0.56	0.82	0.59		z	0.74	0.50	1.83	1.01
	N	x	0.91	0.66	1.37	0.62	N	x	1.02	0.93	1.01	1.16
		y	1.02	0.63	1.90	0.88		y	1.12	1.02	1.87	0.87
		z	0.76	0.52	1.21	0.54		z	0.79	0.47	0.98	0.54
	Stb	x	1.66	1.25	1.82	0.68	Stb	x	1.86	1.39	1.13	0.58
		y	1.70	1.08	2.33	1.28		y	0.96	0.67	2.13	1.09
		z	1.26	0.58	1.36	0.64		z	1.38	0.38	1.55	0.47
Eye	Em l	x	0.34	0.24	0.43	0.34	Em l	x	0.44	0.27	0.48	0.39
		y	0.36	0.32	0.62	0.48		y	0.39	0.30	0.67	0.45
		z	0.19	0.20	0.19	0.16		z	0.30	0.29	0.22	0.21
	Em r	x	0.45	0.37	0.71	0.38	Em r	x	0.58	0.41	0.67	0.76
		y	0.43	0.39	0.55	0.42		y	0.41	0.29	0.62	0.42
		z	0.27	0.32	0.25	0.25		z	0.24	0.23	0.32	0.29
	En r	x	0.58	0.53	0.71	0.67	En r	x	0.88	0.60	0.96	1.12
		y	0.48	0.36	0.74	0.66		y	0.64	0.54	0.74	0.70
		z	0.35	0.25	0.67	0.42		z	0.40	0.30	0.64	0.53
	En l	x	0.62	0.48	0.69	0.81	En l	x	0.96	0.80	0.97	0.25
		y	0.58	0.53	0.86	0.71		y	0.52	0.40	0.85	0.60
		z	0.35	0.27	0.73	0.42		z	0.45	0.33	0.72	0.51
Mouth	Ls	x	0.60	0.53	0.68	0.63	Ls	x	0.51	0.35	0.50	0.43
		y	0.40	0.27	0.54	0.32		y	0.46	0.33	0.67	1.12
		z	0.20	0.19	0.27	0.18		z	0.19	0.16	0.25	0.17
	Li	x	0.58	0.50	0.62	0.25	Li	x	0.44	0.31	0.61	0.54

		y	0.63	0.62	0.80	0.49		y	0.39	0.37	0.45	0.51
		z	0.26	0.27	0.32	0.11		z	0.47	0.09	0.50	0.19
	Sto	x	0.57	0.41	0.62	0.43	Sto	x	0.57	0.52	0.67	0.32
		y	0.71	0.46	0.92	0.69		y	0.46	0.42	0.60	0.29
		z	0.45	0.49	0.39	0.30		z	0.24	0.17	0.27	0.15
	Me	x	0.50	0.37	0.50	0.39	Me	x	0.43	0.30	0.50	0.32
		y	0.79	0.74	1.12	0.77		y	0.61	0.64	0.95	0.64
		z	0.46	0.48	0.73	0.53		z	0.43	0.32	0.48	0.43
	Sl	x	0.46	0.28	0.96	0.56	Sl	x	0.86	0.78	1.25	0.87
		y	0.88	0.55	1.50	1.26		y	0.68	0.51	0.75	0.34
		z	0.76	0.84	0.30	0.28		z	0.49	0.08	0.90	0.36
	Pg	x	0.78	0.58	0.57	0.46	Pg	x	0.80	0.61	0.91	0.84
		y	0.71	0.29	1.36	1.75		y	0.89	0.56	1.47	0.86
		z	0.68	0.29	1.18	0.99		z	0.18	0.15	0.23	0.18
	Sm	x	0.83	0.52	1.55	0.86	Sm	x	0.88	0.65	1.70	0.74
		y	1.28	1.09	0.95	0.81		y	1.30	0.88	0.83	0.60
		z	1.23	1.26	1.89	1.36		z	0.83	0.55	1.41	0.83
	C	x	1.13	0.77	1.14	0.67	C	x	0.98	0.96	1.39	1.00
		y	0.85	0.65	0.92	0.72		y	0.98	0.77	1.35	1.02
		z	1.81	1.04	2.81	1.77		z	1.26	0.72	1.90	0.95
Ear	Pa l	x	0.29	0.22	0.83	0.61	Pa l	x	0.34	0.15	0.55	0.28
		y	0.85	0.64	1.59	1.29		y	1.01	0.91	1.42	0.88
		z	1.04	0.60	1.63	1.20		z	0.84	0.60	1.19	0.69
	Pa r	x	0.18	0.14	0.73	0.49	Pa r	x	0.30	0.30	0.52	0.33
		y	0.84	0.75	2.31	1.10		y	0.91	0.73	1.24	0.68
		z	1.24	0.97	1.51	1.11		z	1.09	0.80	1.43	0.86
	Trg r	x	0.49	0.59	0.82	0.63	Trg r	x	0.36	0.46	0.38	0.26
		y	1.29	0.60	1.45	0.52		y	1.24	0.95	1.53	0.86
		z	1.16	0.69	1.81	0.69		z	0.78	0.45	1.22	0.75
	Trg l	x	0.65	0.50	0.69	0.55	Trg l	x	0.74	0.77	0.33	0.30
		y	1.78	0.78	2.62	1.28		y	1.60	1.26	1.75	1.20
		z	0.94	0.74	2.12	0.80		z	0.90	0.78	1.77	0.98
Other	Tri	x	1.15	0.63	1.20	0.56	Tri	x	1.44	0.76	1.51	0.82
		y	1.78	1.12	1.94	1.12		y	1.75	1.03	1.81	0.96
		z	1.60	1.33	1.70	1.06		z	1.28	0.99	1.40	0.89
	Zy r	x	1.36	0.92	1.73	1.11	Zy r	x	1.22	0.96	1.53	1.00
		y	2.22	1.71	2.40	1.53		y	1.75	1.34	2.02	0.84
		z	1.92	1.32	2.08	1.13		z	1.88	0.80	2.15	1.11
	Zy l	x	1.55	1.12	2.06	1.25	Zy l	x	1.27	1.19	1.59	0.95
		y	1.96	1.10	2.33	1.54		y	1.78	1.29	2.63	0.78
		z	2.33	2.06	2.35	1.27		z	2.16	1.03	2.46	0.72

10 Acknowledgement

I would like to express my special acknowledgment to our Chef and my Doktorvater Univ.-Prof. Dr. Riccardo Giunta and Prof. Dr. Schenck who offered me the precious opportunity to study and pursue the Dr. med in Germany. Thank you for providing me with the great research platform at Ludwig-Maximilians-Universität München and the great opportunity to take part in clinical operations and microsurgery courses in our department at LMU Klinikum. Moreover, your guidance during my studies played a decisive role in starting my career in plastic surgery.

I am extremely grateful to my supervisor, Dr. med. Konstantin Koban. In the past few years, I was involved in many meaningful and interesting research projects we designed. Whenever I had questions or new ideas about my research, you were always available to discuss them with me and gave very constructive advice. It was only with your full support and help that I was able to carry out and completed my doctoral program. Besides the scientific research, you also assisted me in coordinating with other departments and staff in the hospital, so that I could integrate into the group as soon as possible despite my non-proficient German. Your guidance to me is not only limited to scientific research but also sets a model for me as a surgeon and a good person. Working with you is one of my fondest memories.

I would like to give my sincere gratitude to Lucas Etzel, who helped me a lot in the operation and usage of different 3D scanners along with the Vectra 3D imaging system and in the analysis of the 3D models with different software. Those detailed instructions enabled me to start the research quickly. In addition, special thanks to Dr. Frank's efforts

in our joint projects.

I also want to thank the nurses and the secretary in our department, Ms. Haras, Ms. Jerkku, Mr. Pandza, Ms. Penzkofer, Ms. Schweinberger, and Ms. Leutner, for your truly help in daily work.

I am very grateful to China Scholarship Council for the financial support to my doctoral career these years.

Finally, I would like to thank my wife. Your constant encouragement and support have enabled me to overcome difficulties, move forward, and become a better man. Meanwhile, I also want to thank my parents for your continued support throughout my life.

11 Publications:

1. Circ-PTPDC1 promotes the Progression of Gastric Cancer through Sponging Mir-139-3p by Regulating ELK1 and Functions as a Prognostic Biomarker. **Zhouxiao Li**, Ye Cheng, Kai Fu, Qiaowei Lin, Tianyu Zhao, Weiwei Tang, Lei Xi, Lulu Sheng, Hao Zhang, Yangbai Sun. **International Journal of Biological Sciences.** 2021 Oct.

2. Reproducibility of novel soft-tissue landmarks on three-dimensional human facial scan images in Caucasian and Asian. **Zhouxiao Li,** Riccardo Enzo Giunta, Konstantin Frank, Thilo Ludwig Schenck, Konstantin Christoph Koban. ***Aesthetic Plastic Surgery***. 2021 Oct.

3. Xiao Li , Wei Jiang, Yi Zhong, Liangliang Wu, Guoqiang Sun, Hanjin Wang, Jing Tao, **Zhouxiao Li#.** Advances of circular RNAs in thyroid cancer: an overview. ***Biomedicine & Pharmacotherapy***. 2021.Aug.

4. The emerging landscape of circular RNAs in immunity: breakthroughs and challenges. **Zhouxiao Li**, Ye Cheng, Fan Wu, Liangliang Wu, Hongyong Cao, Qian Wang, Weiwei Tang. ***Biomarker research***. 2020.Jul.

5. Overexpression of LncRNA AFAP1-AS1 promotes cells proliferation and invasion in gastric cancer. **Zhouxiao Li,** Zhili Ding, Dawei Rong, Weiwei Tang, Hongyong Cao. ***Oncology letters***. Sep.2019.

6. Single-cell RNA sequencing in cancer: applications, advances and emerging

challenges. Guangshun Sun, **Zhouxiao Li**, Dawei Rong, Hao Zhang, Xuesong Shi, Weijun Yang, Wubin Zheng, Guoqiang Sun, Fan Wu, Xuehao Wang, Yangbai Sun, Weiwei Tang. ***Molecular Therapy—oncolytics.*** 2021 Aug.

7. Xiao Li, Guangshun Sun, Liangliang Wu, Guoqiang Sun, Ye Cheng, Jing Tao, **Zhouxiao Li,** Weiwei Tang, Hanjin Wang. Upregulation of ADAR Promotes Breast Cancer Progression and Serves as a Potential Therapeutic Target. ***Journal of Oncology.*** 2021 Sep.

8. Guoqiang Sun; Dawei Rong; **Zhouxiao Li**; Guangshun Sun; Fan Wu; Xiao Li; Xuehao Wang; Yangbai Sun; Weiwei Tang. Role of small molecular compounds in cancer: Progress, Opportunities, and Challenges. **Frontiers in Cell and Developmental Biology.** 2021. Sep.

9. Up-regulation of SPC25 promotes breast cancer. Qian Wang, Yanhui Zhu, **Zhouxiao Li**, Qian Bu, Tong Sun, Hanjin Wang, Handong Sun, Xiufeng Cao. ***Aging (Albany NY)***. 2019. Aug.

10. Novel insights into circular RNAs in clinical application of carcinomas. Rong D, Tang W, **Li Zhouxiao**, Zhou J, Shi J, Wang H, Cao H. ***Onco Targets Ther***. 2017.Apr.

11. Long noncoding RNA PANDA promotes esophageal squamous carcinoma cell progress by dissociating from NF-YA but interact with SAFA Weihong Shi, Qian Wang, Yonghua Bian, Yanxin Fan, Yang Zhou, Tingting Feng, **Zhouxiao Li**, Xiufeng Cao. ***Pathol Res Pract***. 2019. Oct.

12. Research on the relationship between health literacy and functional exercise adherence in postoperative breast cancer patients. Weiwei Tang, **Zhouxiao Li,** Chongyin Tang, Xiaowei Wang, Hanjin Wang. ***Patient Preference and Adherence***. 2017. Apr.

13. An emerging function of circRNA-miRNAs-mRNA axis in human diseases. Rong D, Sun H, **Li Zhouxiao**, Liu S, Dong C, Fu K, Tang W, Cao H. ***Oncotarget.*** 2017

14. Lucas Etzel, Thilo Ludwig Schenck, Riccardo Enzo Giunta, **Zhouxiao Li**, Ya Xu, Konstantin Christoph Koban. Digital leg volume quantification: Precision assessment of a novel workflow based on single capture three-dimensional whole-body surface imaging. ***Journal of Digital Imaging.*** 2021.Sep.

15. Three-dimensional surface imaging in breast cancer: a new tool for clinical studies? Konstantin Christoph Koban, Lucas Etzel, **Zhouxiao Li**, Montserrat Pazos, Stephan Schönecker, Claus Belka, Riccardo Enzo Giunta, Thilo Ludwig Schenck, Stefanie Corradini. ***Radiation Oncology***. 2020. Feb.

16. Validation of two handheld devices against a non-portable three-dimensional surface scanner and assessment of potential use for intraoperative facial imaging. Konstantin Christoph Koban, Philipp Perko, Lucas Etzel, **Li Zhouxiao**, Thilo Ludwig Schenck, Riccardo Enzo Giunta. ***J Plast Reconstr Aesthet Sur***. 2020. Jan.

17. Whole body surface assessment - implementierung und erfahrungen von 360° 3D ganzkörperscans. Lucas Etzel, Konstantin Koban, **Zhouxiao Li,** Thilo Schenck,

Riccardo Giunta. ***HaMiPla***. 2019. Aug.

18. Precision in 3-Dimensional surface imaging of the face: a handheld scanner comparison performed in a cadaveric model. Koban KC, Cotofana S, Frank Konstantin, Green JB, Etzel Lucas, **Li Zhouxiao,** Giunta RE, Schenck TL. ***Aesthet Surg J***. 2019. Mar.